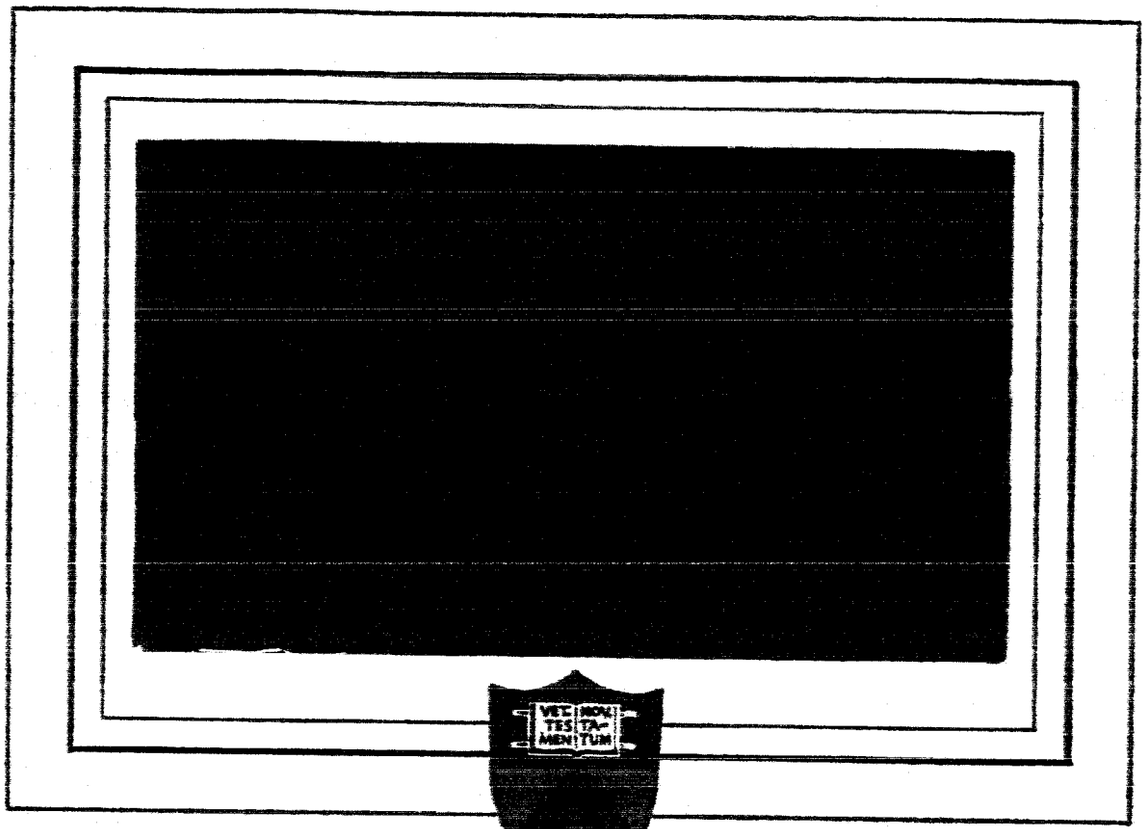

PRINCETON UNIVERSITY

DEPARTMENT OF

AEROSPACE AND MECHANICAL SCIENCES

NATIONAL AERONAUTICS
AND SPACE ADMINISTRATION

Research Grant NsG-306-63

PULSED ELECTROMAGNETIC GAS ACCELERATION

Eighth Semi-Annual Progress Report

1 January 1966 to 30 June 1966

Report No. 634g

Prepared by: R. G. Jahn
Robert G. Jahn
Associate Professor
and Research Leader

and: W. von Jaskowsky
Woldemar F. von Jaskowsky
Research Engineer
and Lecturer

July 1, 1966

Guggenheim Laboratories for the Aerospace Propulsion Sciences
Department of Aerospace and Mechanical Sciences
PRINCETON UNIVERSITY
Princeton, New Jersey

ABSTRACT

Profiles of electric field distribution within the propagating current sheet of a dynamical pinch discharge have been determined by a coaxial double electric probe. The axial electric field component parallel to the sheet, E_z, is found to be essentially that induced by the changing magnetic flux, rather than a resistive potential drop along the sheet column. The radial electric field component, E_r, normal to the sheet, is found to function partly to help accelerate ambient ions to sheet velocity, and partly to drive axial electron current by $E_r \times B_\theta$ drift. By simple analytical models the profile of ion density through the sheet can be computed, and the effective values of the adiabatic exponent, γ, the electron temperature, and the ion temperature at the back of the sheet may be estimated.

An improved piezo-electric pressure probe has been developed which reduces the initial signal risetime below 1 μsec, yet more faithfully reproduces the details of the pressure profile through and behind propagating current sheets after the initial impact signals. High resolution voltage records have been obtained with outer and inner dividers and a "D-loop" which permit evaluation of the very low resistance of the discharge plasma and provide insight into the breakdown initiation mechanism. A gas laser interferometer has been constructed for the purpose of determining the electron density distributions which arise near the current sheets during the pulsed plasma acceleration processes of interest. The microwave reflection interferometer technique has been extended to two complementary modes of operation which yield additional information on these electron density profiles.

Prototype units of low-inductance capacitors suitable for simple, versatile assembly into pulse-line configurations have been constructed, and have performed satisfactorily in initial tests. Construction of the first low-impedance tailored-pulse facility is currently underway.

Studies of the ejection of pulsed plasmas from orifices have been expedited by a large plexiglas exhaust tank, and a mechanized carriage capable of precisely aligning a battery of magnetic probes in the exhaust plume region.

Students Associated With This Program

N. Black	(Graduate Assistant)
A. Bruckner	(Graduate Fellow)
R. Burton	(Graduate Fellow)
C. Carrelli	(Visiting Scholar)
K. Clark	(Graduate Assistant)
K. Cooke	(Graduate Fellow)
A. Eckbreth	(Graduate Assistant)
W. Ellis	(Graduate Assistant)
P. Turchi	(University Scholar)
T. York	(Graduate Assistant)

TABLE OF CONTENTS

LIST OF ILLUSTRATIONS

LIST OF ILLUSTRATIONS - contd.

LIST OF ILLUSTRATIONS - contd.

I. INTRODUCTION

Since the previous semi-annual report,[I-32] we have submitted to the project office a renewal proposal which included a broad review of the research accomplishments of this program since its inception,[I-32] and a lengthy technical report based on the Ph.D. thesis of Dr. Neville A. Black dealing with the dynamics of pinch discharges driven by pulse-forming networks.[I-37] This status report, therefore, will omit both of these topics, and concentrate on other specific studies which have shown progress during the past six months. Some of these are also nearing completion as Ph.D. theses; others are in a phase of data accumulation; still others are only beginning exploratory experiments. Without exception, however, each is designed to answer specific questions regarding pulsed plasma acceleration processes, and each is closely coupled to other studies of the program.

II. ELECTRIC FIELD PROFILES IN THE CURRENT SHEET (Burton)

The previous semi-annual report [I-32] described the measurements of radial and axial electric fields within the current sheets generated in a 5" closed chamber pinch discharge. The experimental data were obtained with an electric field probe discussed in detail therein, which displayed the floating potential difference signal measured by two electrodes immersed in the plasma at a separation of 2 mm. Typical oscilloscope traces are shown in Fig. 1. Point-by-point surveys of the radial and axial electric fields were made in this manner every 1/8", in 10 KV discharges in 120 μ argon. The development of the radial electric field is shown in Figs. 2 and 3. The axial electric field was found to be nearly independent of axial position, and typically resembled that shown in Fig. 1b.

The trajectory of the radial electric field maxima is displayed on a radius-time plot in Fig. 4. After an initial acceleration period, the electric field is seen to convect inward at a constant velocity of 4.3×10^4 m/sec. The maxima in the E field trail slightly behind the maxima in the current density, j, determined in earlier magnetic probe experiments, and the trajectories of E and j agree closely with modified snowplow theory mass and current trajectories.

We can establish that the axial electric field, E_z, is essentially that induced by the changing magnetic flux:

$$E_z = \int_o^r \dot{B}_\theta dr \qquad (1)$$

rather than a resistive drop along the discharge column. Using an inner voltage divider, the resistive drop along the current sheet was found to be about 10 volts/cm, (cf. Sect. IV) whereas the maximum induced E_z reached 450 volts/cm. Figure 5 shows a comparison of the measured E_z profile, with the integrated flux change found from B probe measurements.

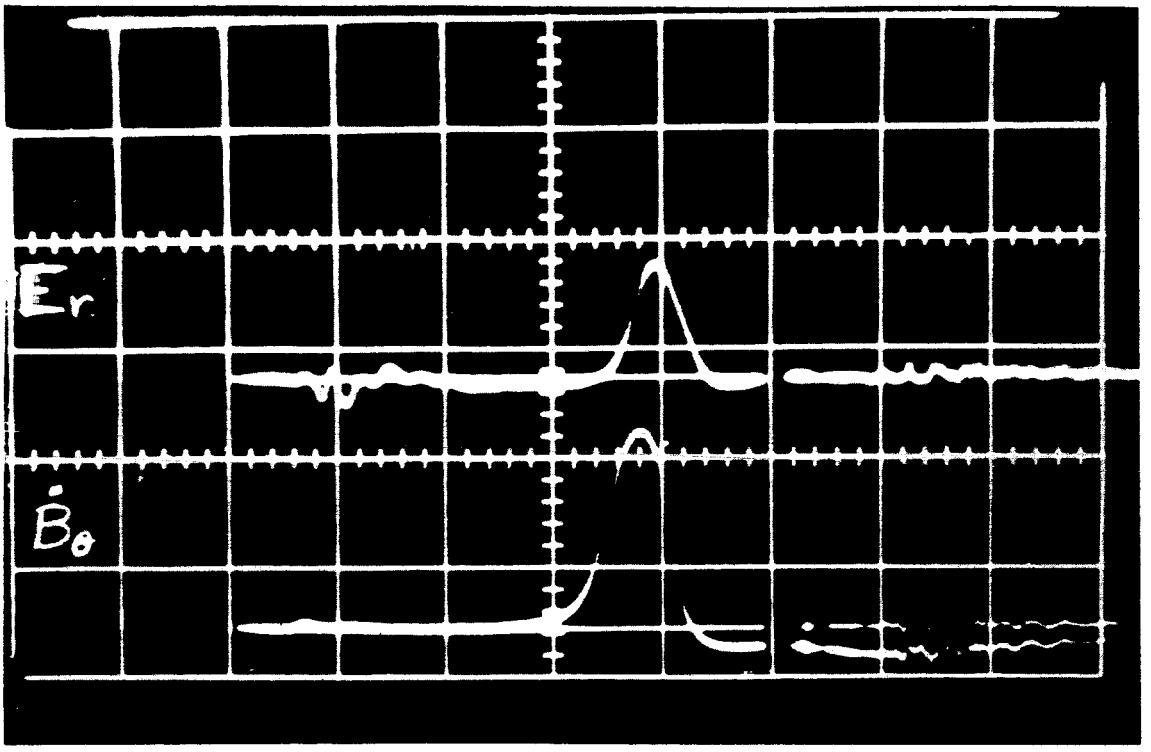

a) SIMULTANEOUS ELECTRIC AND MAGNETIC PROBE RESPONSES, E_r AND $\dot{B}_\theta$
120μ ARGON, 5" CHAMBER, $R/R_0 = .66, z/h = 0.5$

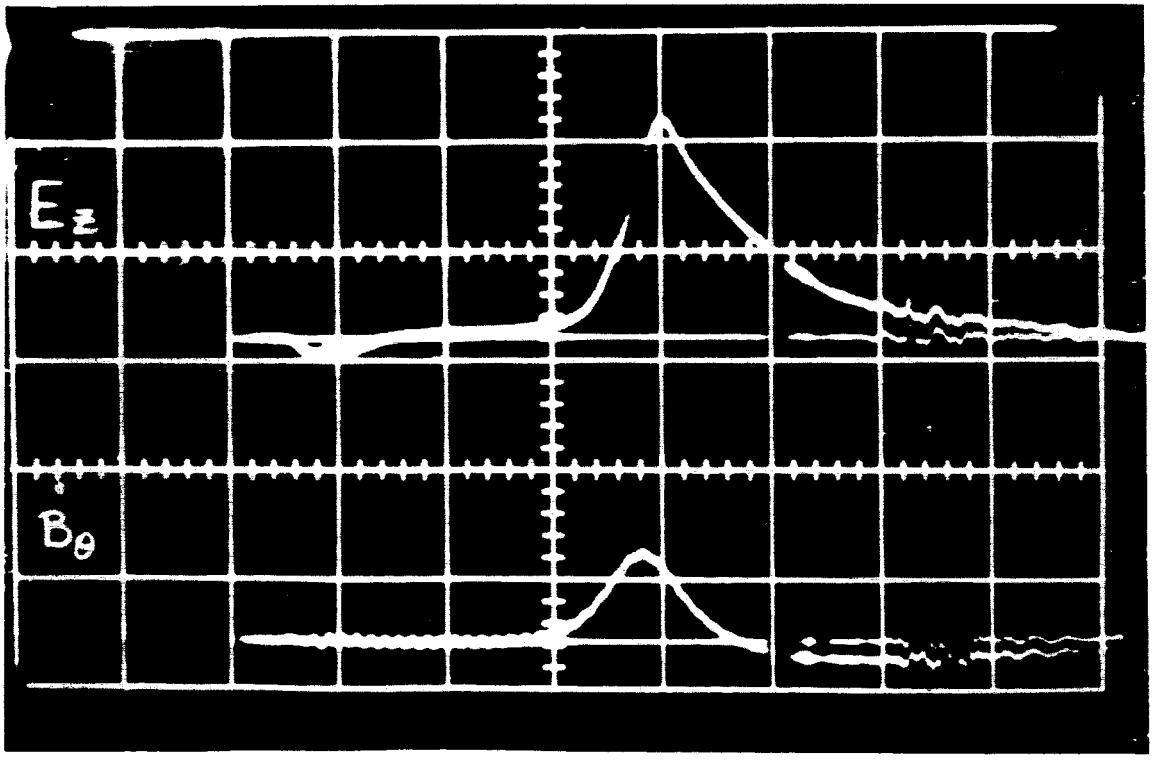

b) SIMULTANEOUS ELECTRIC AND MAGNETIC PROBE RESPONSES, E_z AND $\dot{B}_\theta$
120μ ARGON, 5" CHAMBER, $R/R_0 = .66, z/h = 0.5$

FIGURE 1

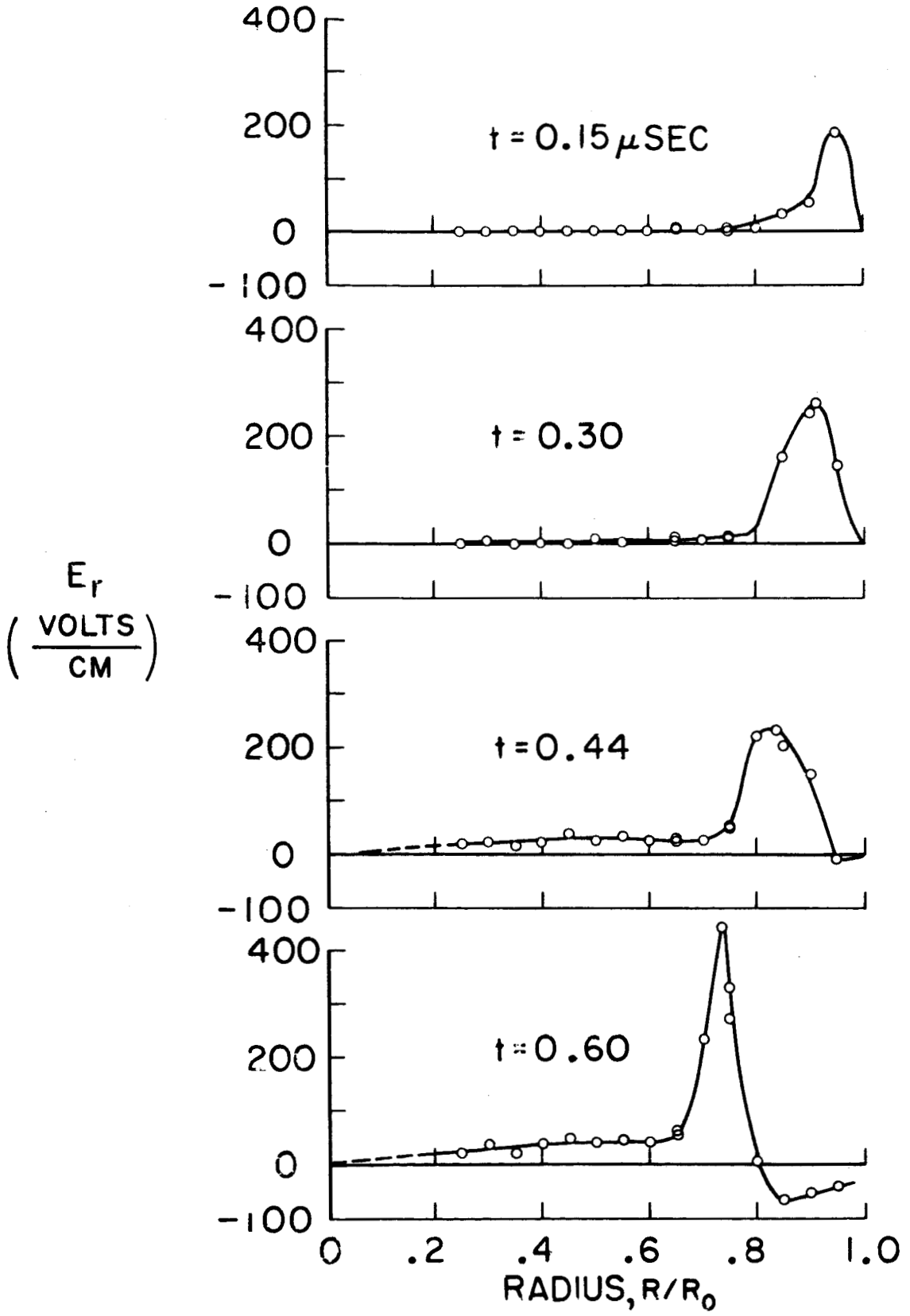

RADIAL ELECTRIC FIELD DISTRIBUTION, $z/h = 0.5$

5" CHAMBER, 120μ ARGON, 10 KV

FIGURE 2

AP25-4088-66

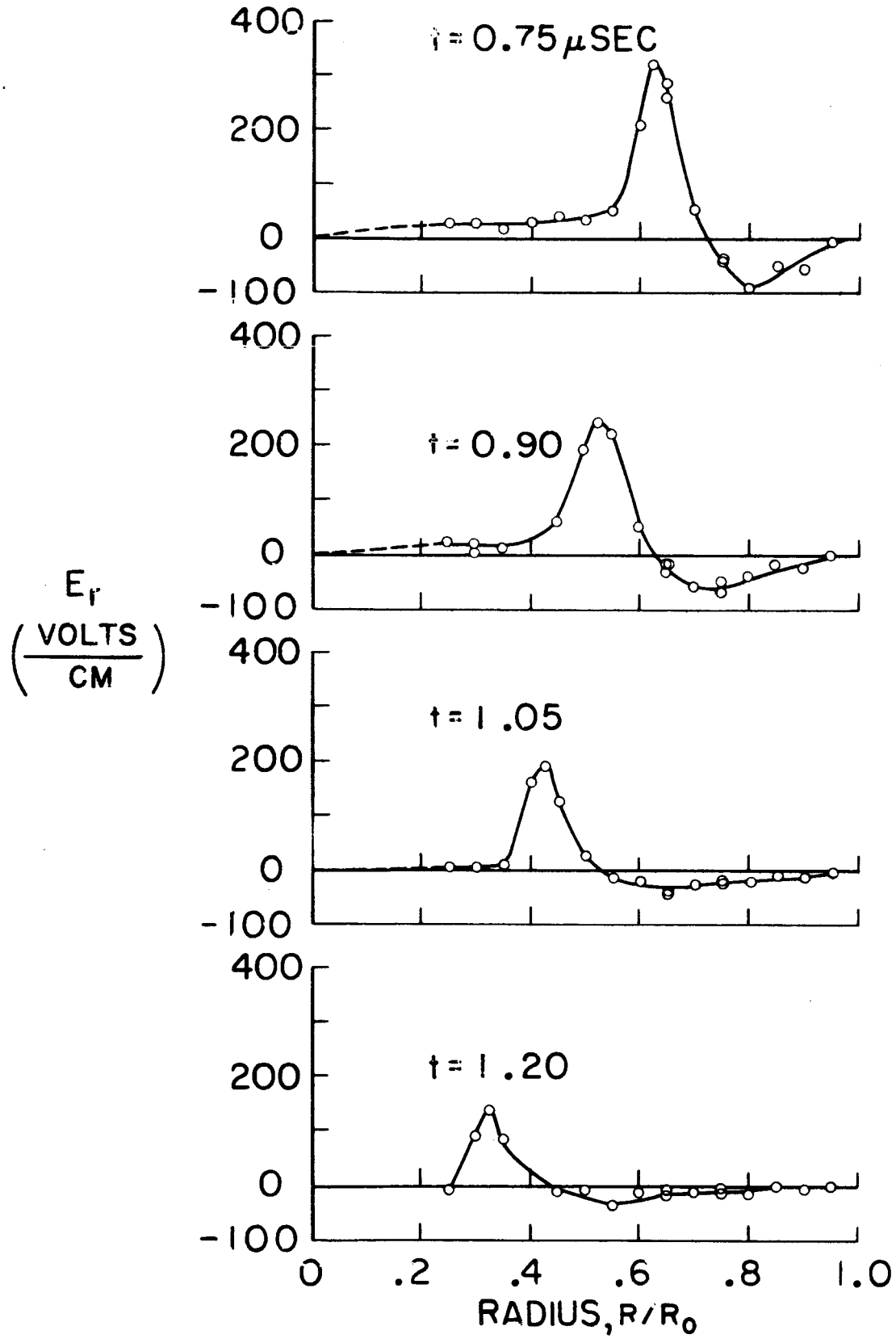

RADIAL ELECTRIC FIELD DISTRIBUTION, z/h = 0.5

5" CHAMBER, 120 μ ARGON, 10KV

FIGURE 3

AP25-4089-66

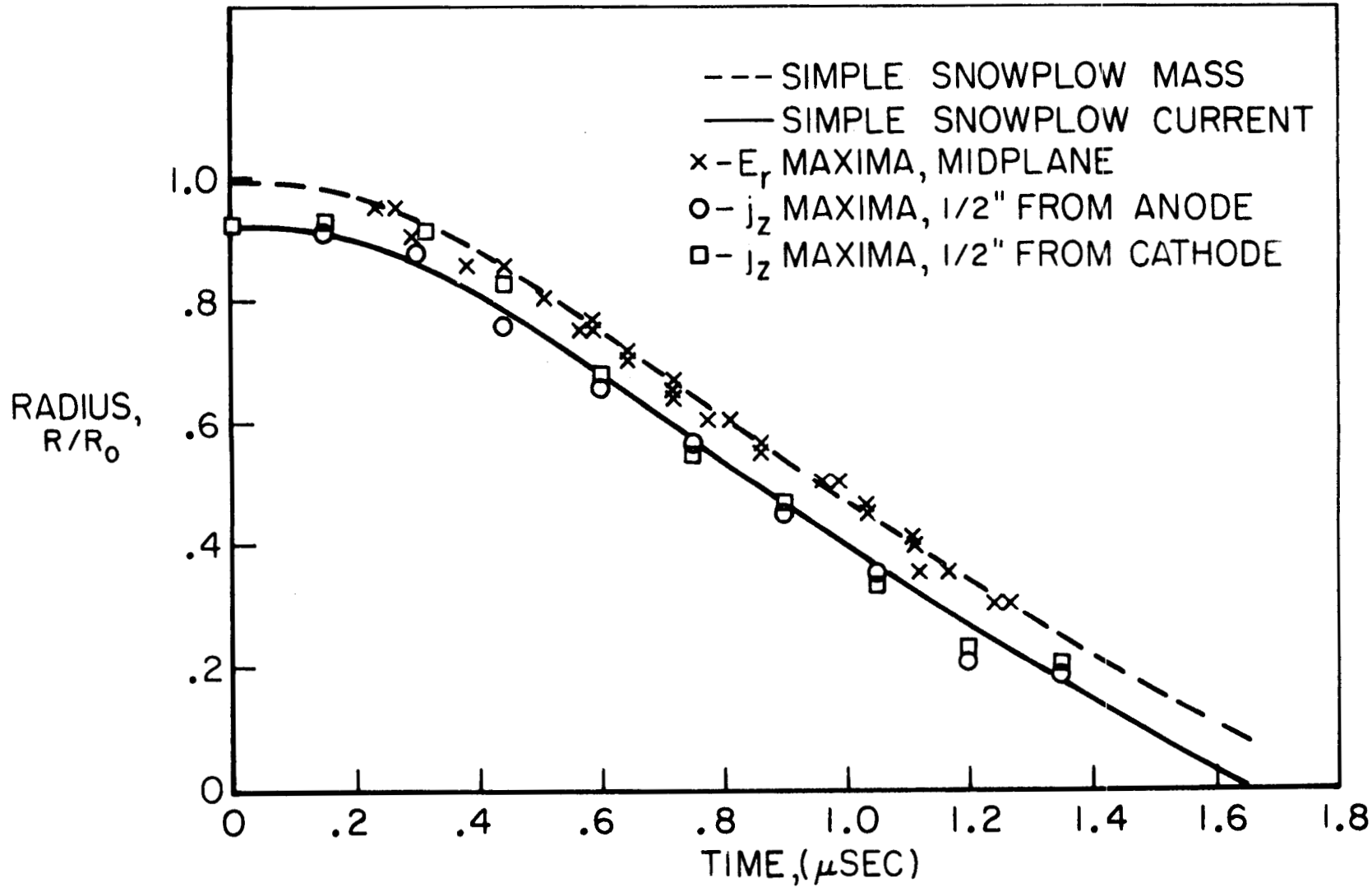

FIGURE 4

SNOWPLOW, AXIAL CURRENT, & RADIAL ELECTRIC FIELD TRAJECTORIES

5" CHAMBER, 120μ ARGON, 10KV

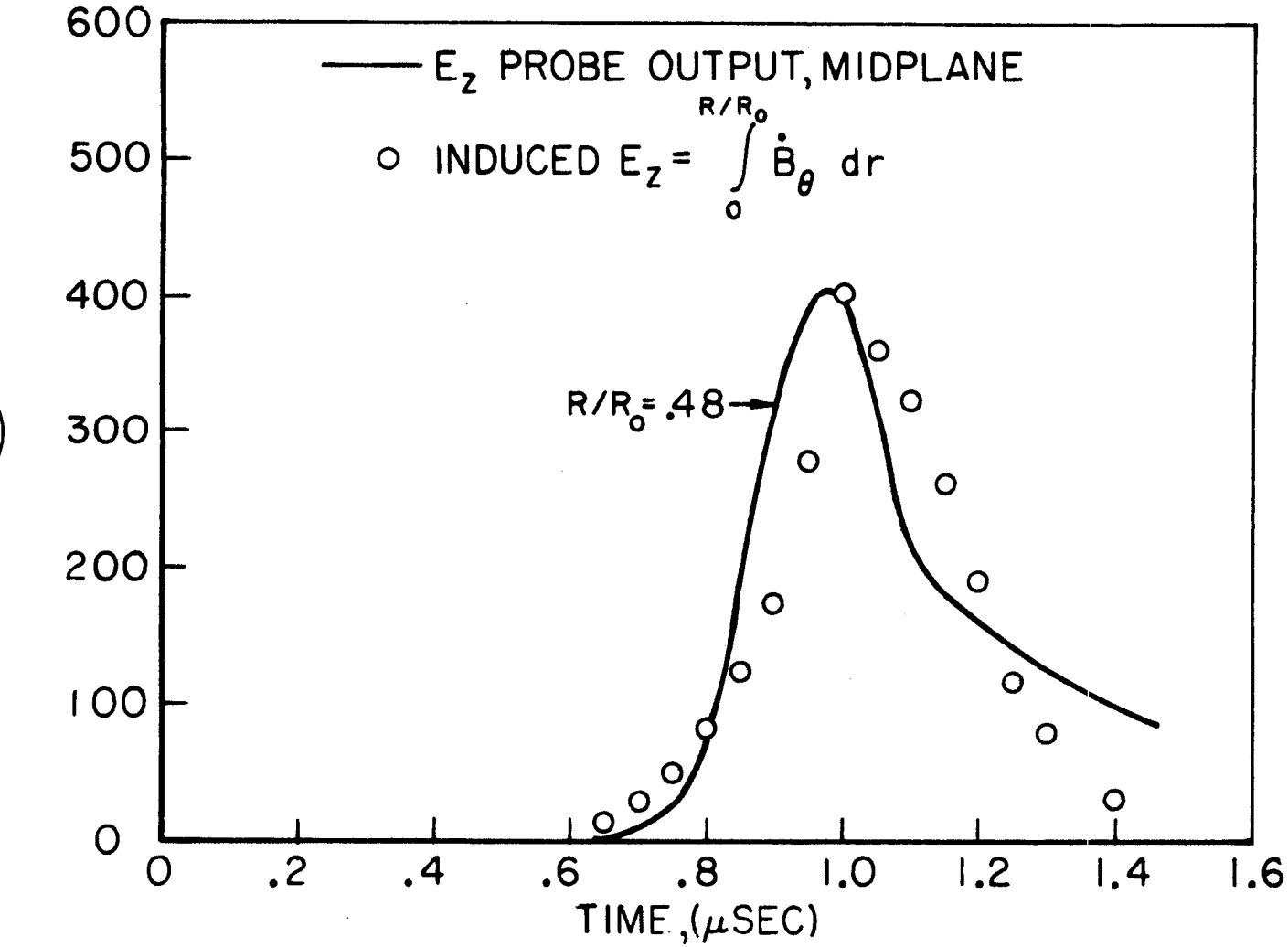

FIGURE 5

AXIAL ELECTRIC FIELD FROM ELECTRIC & MAGNETIC PROBES

To the approximation that E_z is established solely by $\dot{B}_\theta$, it follows that in a coordinate system moving along with the current sheet, since $\dot{B}_\theta$ is zero, E_z will also be zero, and the total electric field is purely radial (see Fig. 6).

It is possible to illustrate the origin and function of the radial electric field in the current sheet by reference to a simplified magnetogasdynamic model. In the reference frame moving with the current sheet, neutrals stream into the sheet from the left at velocity U_s. At the leading edge of the sheet, the electron temperature rises abruptly to a value adequate to ionize the particle stream completely, leaving a stream of ions and electrons of equal density $n_+ = n_e = n$. Since the electron Hall parameter, Ω , is larger than unity in this environment, the electrons will gyrate in the perpendicular E_r and B_θ fields (Fig. 6), conducting an axial current in accordance with Ohm's Law[I-41]:

$$j_z = \sigma_o \frac{E_r}{\Omega} = \left(\frac{ne^2}{m\nu_c} \right) \frac{E_r}{\Omega} = ne \frac{E_r}{B_\theta} \qquad (2)$$

Note that the axial electron current is independent of collision frequency ν_c.

Equation (2) is the statement that the axial current is conducted by electrons in $\vec{E} \times \vec{B}$ drift, independent of the value of Hall parameter Ω . The equation can also be rearranged to show that the force on the electrons, $j_z B_\theta$, is equal to the force on the ions, enE_r. Furthermore, from Eq. (2) one may calculate the particle density n, from measured values of j_z, B_θ, and E_r. A typical density profile is plotted in Fig. 7, normalized to ambient density n_A , at 120 μ argon. The density ratio rises steadily through the sheet, reaching a compression ratio of about 6 at the point of maximum electric field. This calculation is accurate to within about 25 percent at the front and center of the current sheet, since the accuracy is limited only by the experimental measurement of B_θ and E_r . Moving

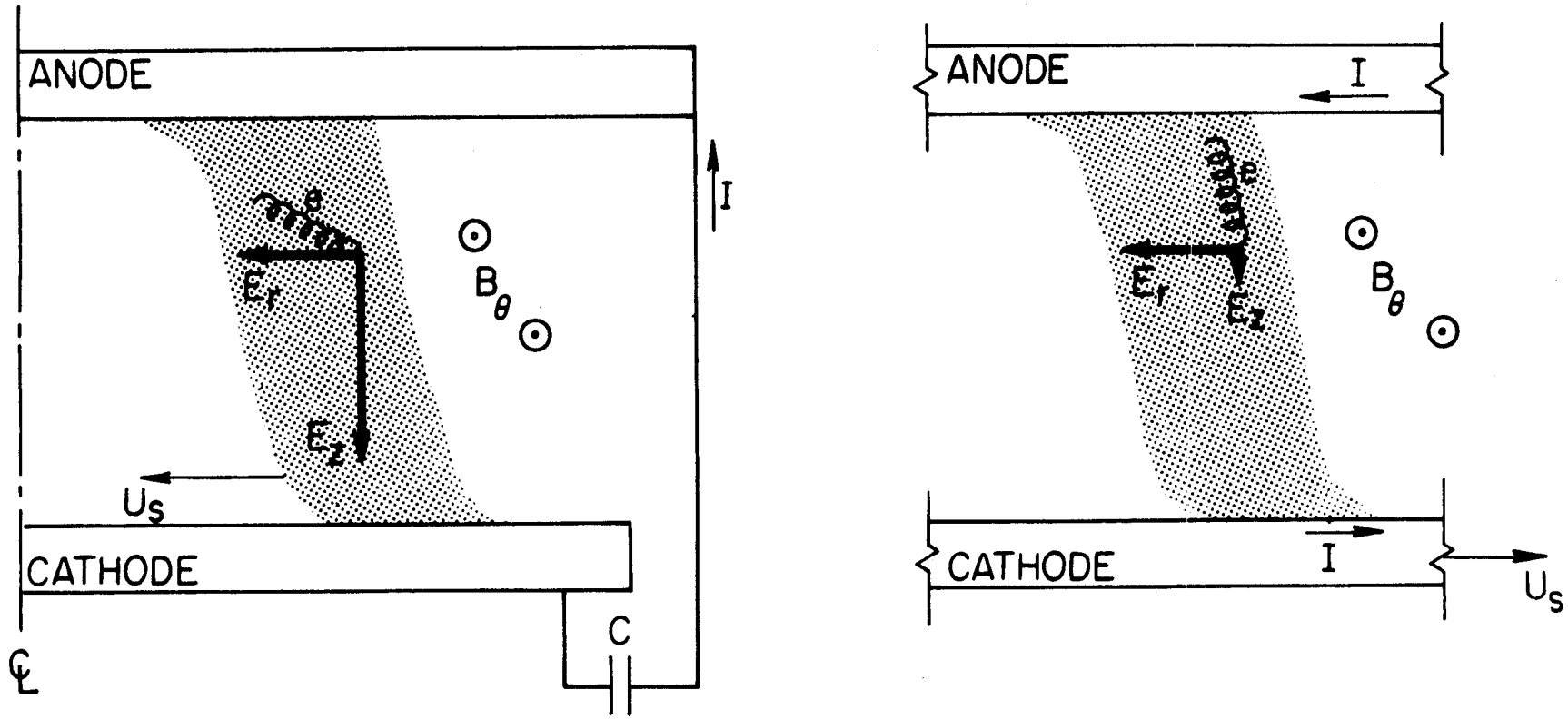

LABORATORY COORDINATES

MOVING COORDINATES

FIGURE 6

ELECTRIC FIELD COMPONENTS & ELECTRON $\vec{E} \times \vec{B}_\theta$ DRIFT

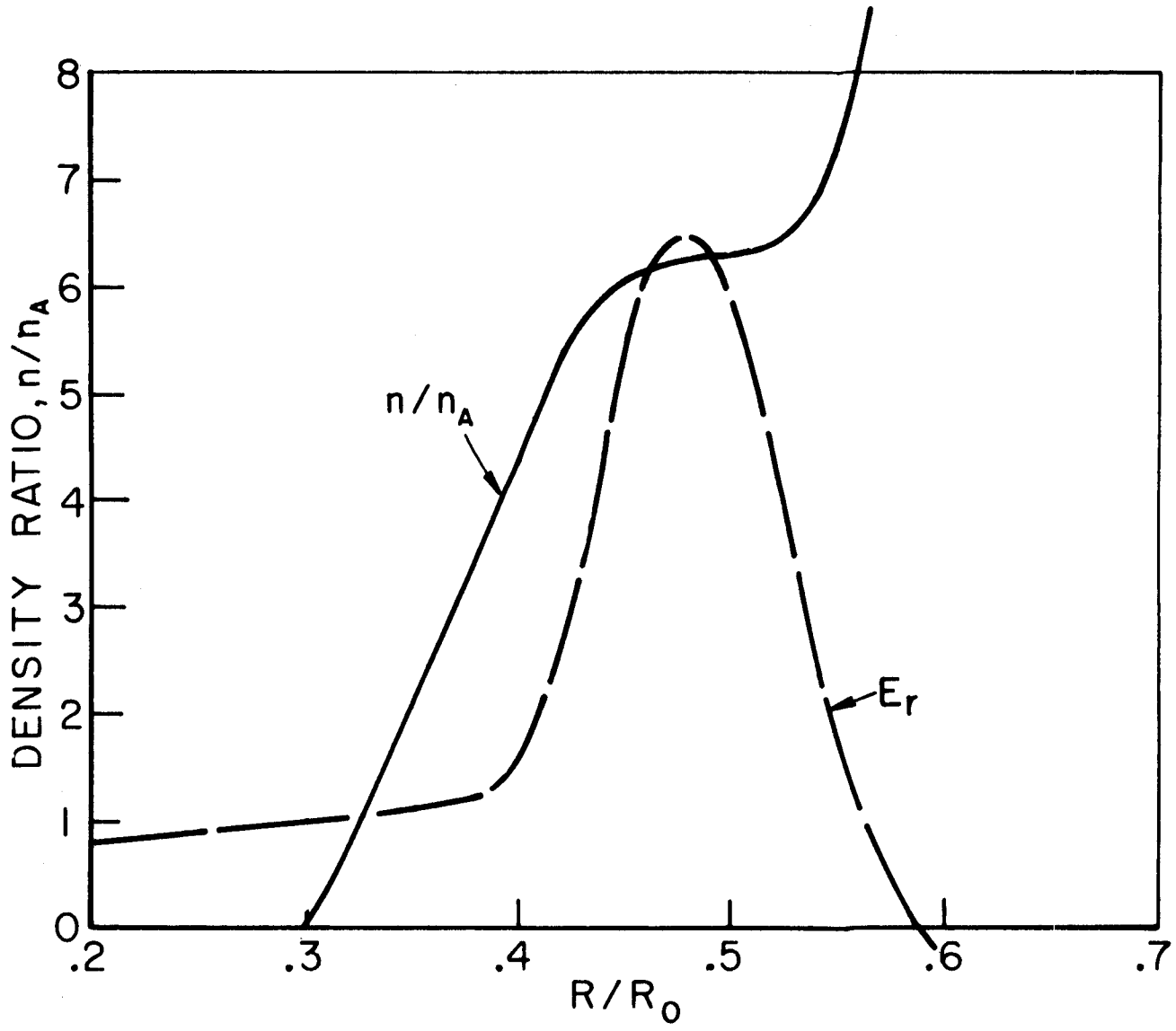

PARTICLE DENSITY VS RADIUS IN 5" PINCH
120μ ARGON, 10KV, t = .95 μsec

FIGURE 7

further back in the sheet, however, the E_r field deviates strongly from the value it would have had in a truly one-dimensional current sheet. Specifically, the effect of finite radial current density causes E_r to reverse sign at the back of the sheet, and Eq. (2) is not valid in this region.

A second estimate of the profile of density, n(r) through the sheet may be made from the radial component of Ohm's Law:

$$j_r = \sigma_o \left[\frac{1}{1+\Omega^2} E_r + \frac{\Omega}{1+\Omega^2} UB_\theta \right] \qquad (3)$$

From axial B probe surveys, we have found that the radial current density is nearly zero, and to this approximation,

$$E_r = -\Omega UB_\theta \qquad (4)$$

Substituting Eq. (4) into Eq. (2),

$$j_z = -\sigma_o UB_\theta \qquad (5)$$

To estimate U from measured values of j_z and B_θ, we need to estimate the scalar conductivity, σ_o. For a Maxwellian electron swarm in a neutral plasma where Coulomb collisions predominate, σ_o is independent of electron density, and may be written: [I-41]

$$\sigma_o = .55 \times 10^4 \, (T_e[\text{e.v.}])^{3/2} \text{ mhos/m} \qquad (6)$$

Relating j to B by Maxwell's equation, and U to n(r) by continuity (Eq. 8) we have

$$\frac{n_A}{n(r)} = \frac{r}{r_s U_s \sigma_o \mu_o Br} \frac{dBr}{dr} = 145 \frac{r}{r_s U_s} T_e^{-3/2}[\text{e.v.}] \frac{d(\ln Br)}{dr} \qquad (7)$$

In regions of the plasma where T_e is a constant, Eq. (7) states that n(r) is inversely proportional to a logarithmic derivative, which can be evaluated to 20 percent accuracy from experimental magnetic probe data. Several processes compete to change electron temperature however, and it is not expected

that T_e will remain constant through the sheet. Through detailed thermodynamic and gas kinetic arguments,[I-41] it can be established that the electron temperature within the sheet must be of the order of a few electron volts, the point at which the energy loss by inelastic collisions, thermal conduction, and radiation, balances the power input by ohmic heating. The sensitivity of the calculation of $n(r)/n_A$ to the profile of T_e may be inferred from Fig. (8), where $n(r)/n_A$ is plotted for two cases of assumed temperature profiles. In the first case, T_e assumes a constant value of 1.1 e.v. throughout the sheet. This particular value is calculated directly from Eq. (7) at the leading edge of the sheet, where the density ratio is assumed to be unity. In the second case, which more realistically approximates the actual temperature profile, T_e rises smoothly from 1.1 e.v. to a maximum of 3 e.v. at the sheet center, returning to 1.1 e.v. at the rear edge. Also included for comparison in Fig. (8) is the profile $n(r)/n_A$ from Fig. (7).

Because the current sheet is efficiently sweeping up and accelerating mass as it propagates inward, the density profile in the sheet is necessarily an unsteady one. To formulate a model of this unsteady process, one may envisage two alternate methods for storing the accumulated mass. In the first, the sheet volume remains constant, and incoming particles are stagnated in a reservoir of increasingly higher density. In the second, the sheet behaves like a strong, albeit thick, gasdynamic shock. Fluid passing through the sheet is accelerated to a large fraction of sheet velocity, and is compressed to a constant high density behind it, where it is stored in a region of increasingly larger volume. In both of these models the compressive effect due to the cylindrical geometry must be included.

Unfortunately, the correct choice between these two unsteady models cannot be made on the basis of present

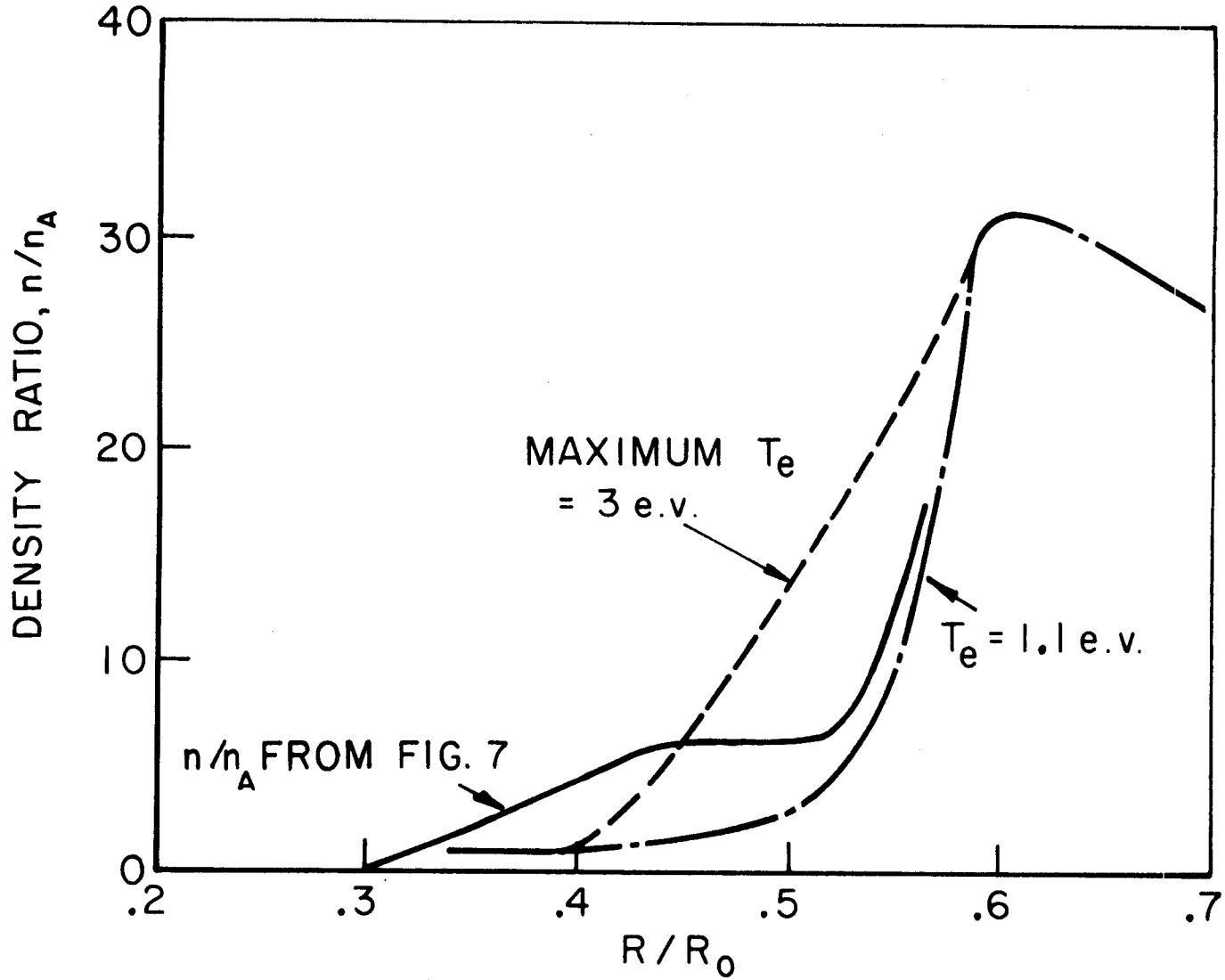

PARTICLE DENSITY RATIO VS RADIUS IN 5" PINCH,
120μ ARGON, 10KV, t = .95μsec

FIGURE 8

experimental evidence. The difference between the constant volume and constant compression models will most readily manifest itself in a measurement of the time history of the density at the back of the sheet, or of the thickness of the high density region, and measurements of this type have proven extremely difficult. Lacking any experimental indication of the more proper point of view, the constant compression model has been adopted arbitrarily, largely because it has the virtue that the density profile becomes steady in the reference frame of the current sheet, over propagation distances small compared with the radius.

From this point of view it is then reasonable to write "jump conditions" across the entire sheet, and for propagation distances small compared with the sheet radius, to view the sheet as a steady, one-dimensional, dissipation zone. These conditions may be derived from the differential form of the equations of motion:

$$\frac{dnU}{dx} = 0 \tag{8}$$

$$\rho U \frac{dU}{dx} + \frac{dp}{dx} + \frac{1}{2\mu_o} \frac{dB^2}{dx} = 0 \tag{9}$$

$$\rho U \frac{d}{dx} \left(C_p T + \frac{1}{2} U^2\right) = j \left[\frac{1}{\sigma_o} j + UB\right] + \frac{d}{dx} \left(K \frac{dT}{dx}\right) \tag{10}$$

provided each term can be written as an exact derivative. The only troublesome term is that in brackets in the energy Eq. (10). However, this term contains the difference between ohmic heating and work done on the fields by the plasma, and is identically zero by Eq. (5). Integrating across the shock, we have:

$$n_1 U_1 = n_2 U_2 \tag{11}$$

$$\rho_1 U_1^2 + p_1 + \frac{1}{2\mu_o} B_1^2 = \rho_2 U_2^2 + p_2 + \frac{1}{2\mu_o} B_2^2 \tag{12}$$

$$C_p T_1 + \frac{1}{2} U_1^2 = C_p T_2 + \frac{1}{2} U_2^2 \qquad (13)$$

divide the momentum equation by $\rho_1 U_1^2$, the energy equation by $(1/2) U_1^2$ and neglect the terms p_1, $\frac{1}{2\mu_o} B_1^2$, and $C_p T_1$, we find:

$$\frac{P_2}{\rho_1 U_1^2} = 1 - \frac{n_1}{n_2} - \frac{\epsilon}{2} \qquad (14)$$

$$\frac{2C_p T_2}{U_1^2} = 1 - \left(\frac{n_1}{n_2}\right)^2 \qquad (15)$$

The parameter ϵ in Eq. (14) is the ratio of magnetic energy density to streaming kinetic energy density, $B_2^2/\mu_o \rho_1 U_1^2$, and has a measured value of 1.33. (In the snowplow theory, $n_1/n_2 = 0$, $p_2 = 0$, and $\epsilon = 2$.) In the present experiment, since the compression $n_2/n_1 >> 1$, we may combine Eqs. (14) and (15), assuming $p = nkT$, to give,

$$1 - \frac{\epsilon}{2} \approx \frac{k}{2m_+ C_p} \frac{n_2}{n_1} \qquad (16)$$

We may view Eq. (16) as a requirement for a constant velocity current sheet. If ϵ is greater than 2, for example, the equation cannot be satisfied, and the current sheet will accelerate. As ϵ approaches 2, the average specific heat C_p must be very large if the sheet is to have constant velocity. In the present experiment, $\epsilon = 1.33$; thus to conform to the observed constant velocity, we must require $\frac{k}{2m_+ C_p} \frac{n_2}{n_1} = .33$. For example, for $n_2/n_1 = 10$, $C_p = 3.1 \times 10^3$ joule/kg°K (corresponding to $\gamma = \frac{C_p}{C_v} = 1.07$). Inserting this value in Eq. (15) yields an ion temperature at the rear of the sheet, $T_2 = 28$ e.v. Note that this ion temperature is one order

of magnitude larger than T_e, and thus the ions can heat electrons in the sheet.

As yet we have not attempted to relate the electric field to other properties of the sheet. Combining Eqs. (2) and (5):

$$E_r = - \frac{j_z^2}{\sigma_o} \frac{1}{en_A U_s} \text{ volts/meter} \qquad (17)$$

Thus the radial electric field is proportional to the axial ohmic heating, and inversely proportional to the radial ion current, which by continuity is constant through the sheet. From measured values of E_r and j_z we may calculate σ_o, and hence the electron temperature. At the maximum in the current density, we calculate $\sigma_o = 2.1 \times 10^4$ mhos/m and hence $T_e = 2.5$ e.v., confirming our earlier assumption.

Integrating Eq. (17) through the sheet, and multiplying by the sheet frontal area, we may find the total ohmic heating within the sheet:

$$\int \frac{j^2}{\sigma_o} dV = - en_A U_s (2\pi rh) \int Edr \quad \text{[watts]} \qquad (18)$$

Over much of the chamber the integral $-\int Edr$ is measured to be about 200 volts. At a radius of 5 cm., the joule heating rate is then 90 megawatts, compared with the maximum power input to the chamber of over 700 megawatts.

The detailed derivation and results of the analytical model sketched here, along with a complete description of the electric and magnetic field mapping experiments are presented in a forthcoming Ph.D. thesis by R. L. Burton.[I-41]

III. PRESSURE MEASUREMENTS IN CLOSED CHAMBER DISCHARGES (York)

The general technique of piezoelectric probing of the pressure in a closed chamber pinch discharge and some preliminary experimental results were presented in the previous semi-annual report.[I-32] It was reported that a piezoelectric probe with a sufficiently fast risetime (approximately 1 μsec) had been constructed but that internal stress wave oscillations were present and had a deleterious effect on the probe response after pressure pulse arrival was sensed. The actual response of this probe to a reflected shock wave in a shock tube and to a current sheet in the closed pinch chamber were displayed. Since that time, both initial and long-time probe response have been substantially improved by development of a "tailored-performance" probe, described below.

In a first effort to improve the fidelity of the probe response, the brass backing rods previously used were replaced by materials more closely matching the acoustic impedance of the PZT-5 crystal elements. Surprisingly, the results were no better than with the brass, suggesting that the degree of wave reflection at the crystal-rod surface was insensitive to the backing rod mismatch. Rather, it was found far more important to suppress sympathetic radial crystal oscillations by matching Poisson's ratio between the crystal and the backing rod. Stainless steel was found to be the most reasonable match for PZT-5 in this regard, and studies revealed that variation of the crystal-backing rod diameter had significant effect on the radial oscillations. Largely by trial and error a 5/32" size was selected as optimum. Finally, the material bonding the sides of the crystal was also found to play a role, and the best compromise here was found to be Apiezon putty.

The improvements derived from these studies were incorporated in one probe (#1), and the performance determined by examining its response to a reflected shock wave (Fig. 9a-f). These records show probe response to a reflected shock in a 7/8" diameter shock tube with a 21-3/4" helium filled driver and a 20-3/4" driven section filled with air, both at room temperature. Figure 9a shows the time interval of primary interest, and reveals that the onset of the radial oscillation has been delayed until approximately 1.5 μsec. The other records display successively longer time intervals which indicate the faithfulness of reproduction of the probe to the complete pressure history.

In order to make pressure measurements in the pinch chamber, it is necessary to insulate the crystal surface from the discharge. This insulation is probably the most critical aspect in the construction of the gauge. On the basis of a number of tests with both thin tapes and lacquers, a reasonably satisfactory covering was found to be provided by one layer of Scotch Brand Polystyrene Type (#74, 1 mil thick) and several coats of Zapon lacquer. It was experimentally determined that this covering produced no noticeable delay or dispersion of the pressure pulse. The response of a probe (#2) with this covering to a reflected shock wave is shown in Fig. 10a.

This insulated probe was next inserted into the 8" diameter pinch chamber flush with the cathode surface. A magnetic probe was also mounted in the sides of the nylon holder of the pressure probe, perpendicular to the plane of the electrode, and positioned to measure $\dot{B}_\theta$ (Fig. 11). The pressure sensing crystal was of 5/32" diameter, the magnetic probe was of 3/32" i.d. A series of simultaneous measurements of $\dot{B}_\theta$ and pressure at various radii in a 100 μ argon discharge driven by a 5 usec rectangular pulse are presented in Fig. 10 b-e. It can be seen that in all cases a large

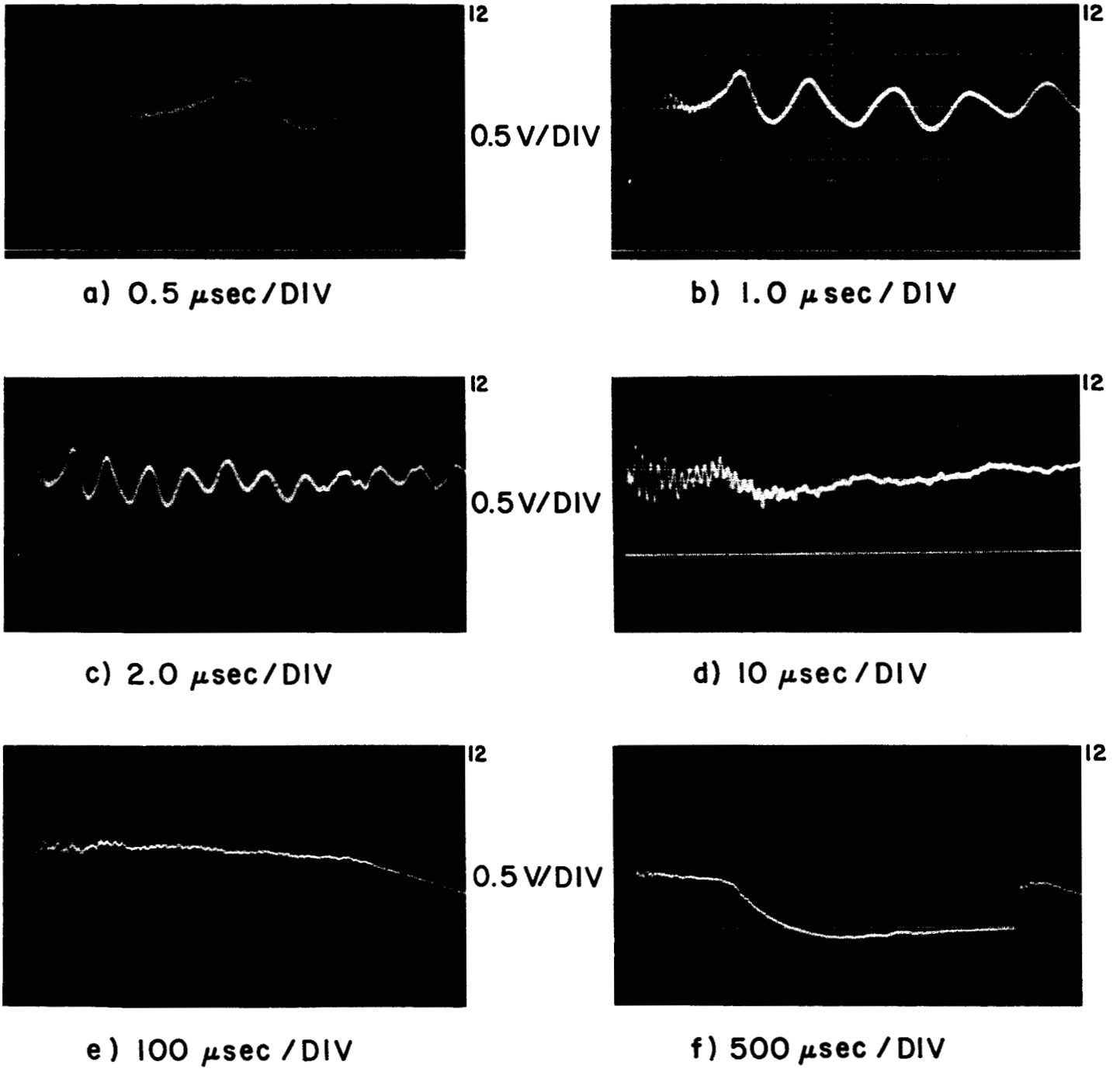

PRESSURE PROBE RESPONSE TO A REFLECTED SHOCK IN SHOCK TUBE

FIGURE 9

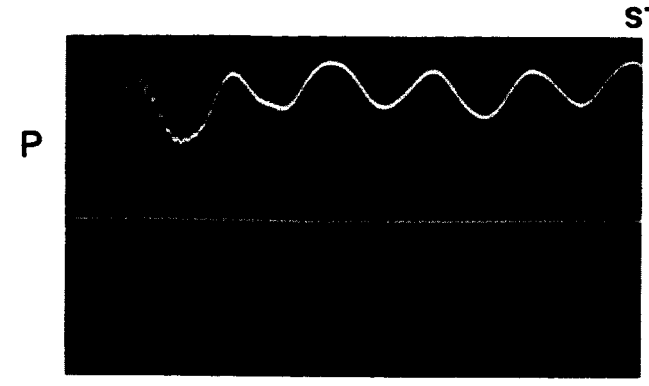

a) RESPONSE OF INSULATED PRESSURE PROBE TO A REFLECTED SHOCK

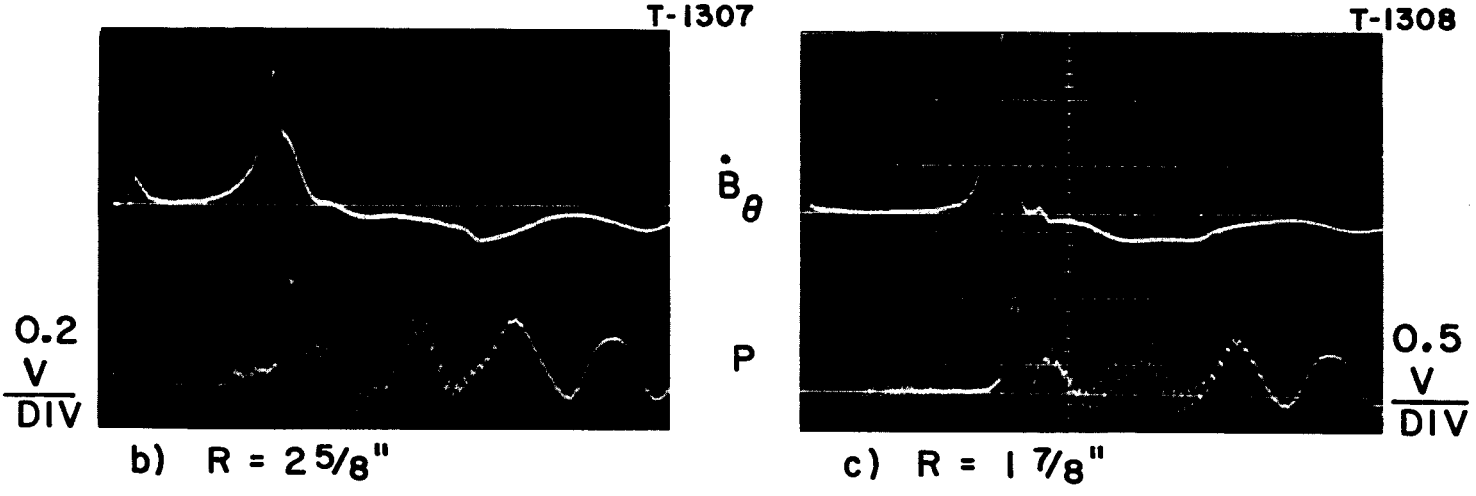

b) R = 2 5/8"

c) R = 1 7/8"

(TIME SCALE : 1 μ sec / DIV)

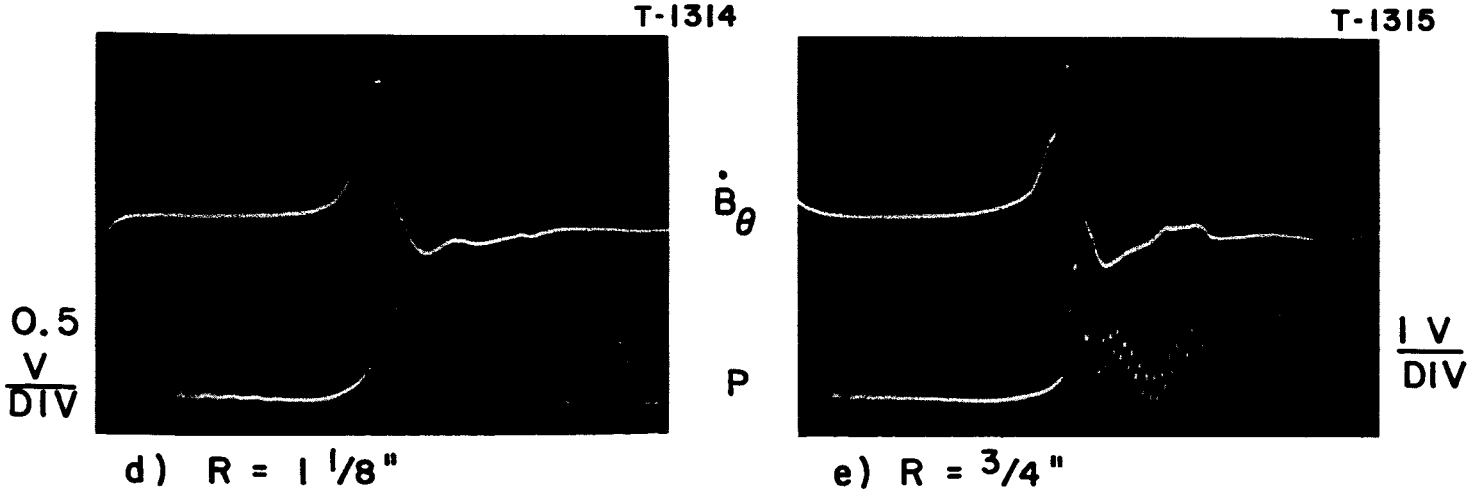

d) R = 1 1/8"

e) R = 3/4"

(b) – (e) : SIMULTANEOUS MEASUREMENTS OF $\dot{B}_\theta$ AND PRESSURE AT VARIOUS RADII

AP25-P620-46

FIGURE 10

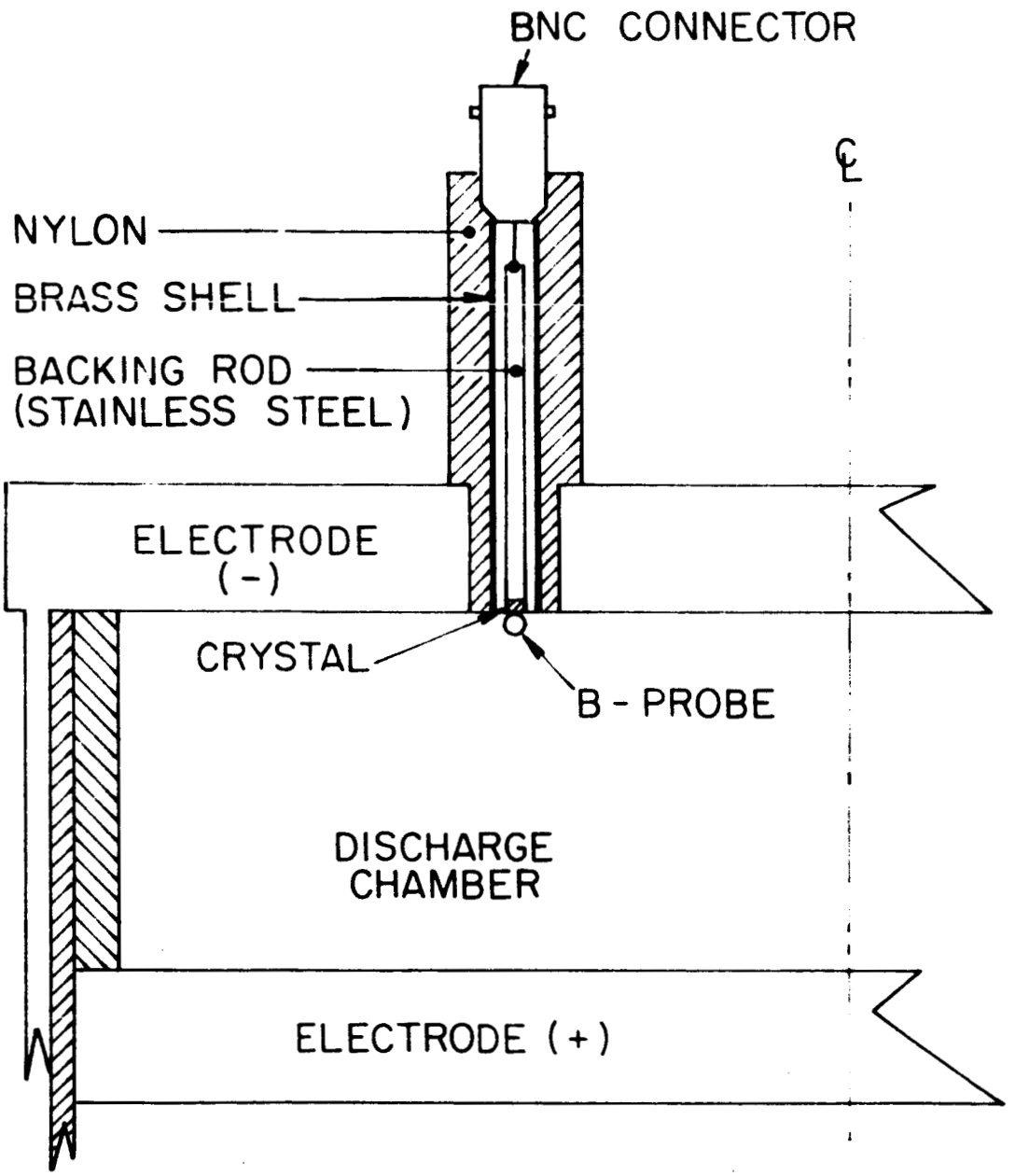

PRESSURE AND MAGNETIC PROBE UNIT IN 8"
DISCHARGE CHAMBER (SCHEMATIC)

AP25-4177-66

FIGURE 11

positive pressure jump arrives almost simultaneously with the $\dot{B}_\theta$ peak, followed by a negative pressure drop of comparable magnitude. The signals following this drop correspond to radial "ringing" of the probe, but are centered about a relatively low pressure. The indication is thus that the current sheet is entraining a large fraction of the ambient gas.

Present efforts are being directed toward eliminating extraneous signals through the pressure probe insulation so that a complete survey of pressures within the closed chamber pinch discharge can be made under various experimental conditions. Further, the detailed effects of the magnetic probe on the pressure gauge response are being examined in order that significant correlation of these two variables can be made.

IV. VOLTAGE SIGNATURES FROM PULSED PLASMA DISCHARGES (Carrelli)

High resolution voltage records have been obtained across a 5" pinch machine for the double purpose of identifying the resistive and the inductive components of the plasma load on the supply, and of contributing some insight on the nature of the mechanisms which initiate the breakdown. The discharge is driven by a 10 KV 15 μF capacitor bank, and argon pressures from 15 to 1600 μ have been studied. The 5" apparatus has been completely described elsewhere, but it is worthwhile to recall certain of its critical features. The chamber itself is formed by two circular plane aluminum electrodes separated by a two-inch gap for test gas and a glass ring insulator 7 mm thick (Fig. 12). A resistor keeps the electrodes at the same potential before the breakdown of the gas, and then plays a negligible role during the main discharge. The pinch chamber is connected to the capacitor bank through a low inductance switch, in such a way that the overall inductance of the circuit is of the order of 10^{-9} - 10^{-8} henries. Hence the ringing frequency is roughly 450 KC. The maximum value of the current is 3×10^5 Amp. All of the voltage measurements are taken with a Tektronix voltage probe type P6013 connected directly to a Type L preamp of a 551 Tektronix scope.

The total voltage across the chamber may be written: (see Figure 12)

$$V_{ch} = \frac{d\phi_p}{dt} + \frac{d\phi_{in}}{dt} + \left(\frac{R_p R_{res}}{R_p + R_{res}}\right) I \qquad (19)$$

where $\frac{d\phi_p}{dt}$ is the variation of the flux linked by the plasma sheet. If we identify a plasma inductance, L_p, then

$$\frac{d\phi_p}{dt} = L_p \frac{dI}{dt} + I \frac{dL_p}{dt} \qquad (20)$$

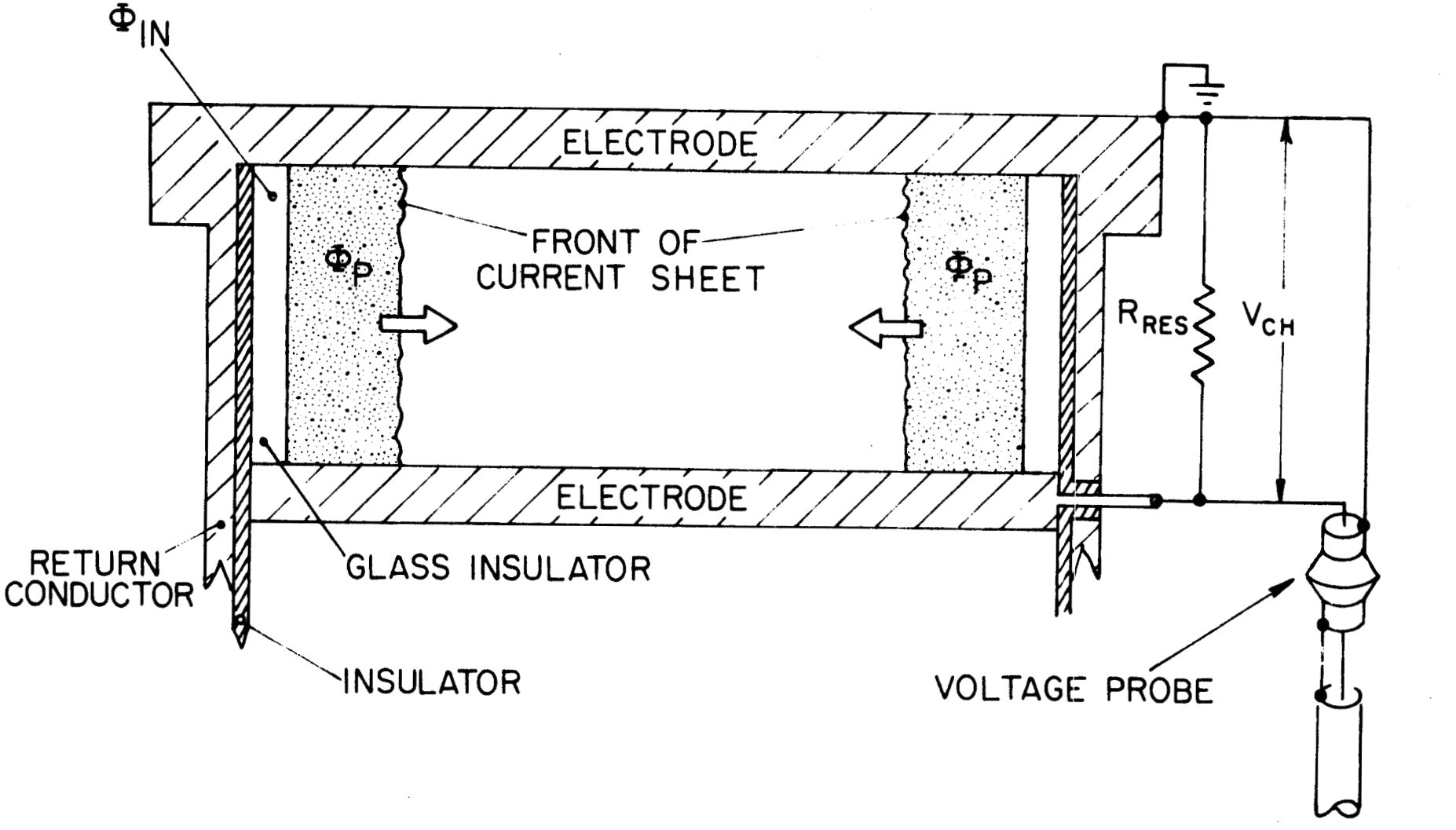

DISCHARGE CHAMBER (SCHEMATIC)

FIGURE 12

The term $\frac{d\phi_{in}}{dt}$ in (19) is the variation of the flux linked by the insulating glass ring and may be represented by a fixed inductance L_{in}:

$$\frac{d\phi_{in}}{dt} = L_{in} \frac{dI}{dt} \tag{21}$$

R_p denotes the resistance of the plasma, and R_{res} the resistance of the external resistor across the chamber. Note that the overall voltage contains four terms, two of which are in phase with the current $\left(\frac{R_p R_{res}}{R_p + R_{res}} + \frac{dL_p}{dt}\right) I$ and two leading it by about 90 degrees. In Fig. 13 a typical voltage trace is compared to the current and to its derivative.

In order to separate the resistive component and the contribution from the change of flux in the insulator glass ring to the overall voltage, two other types of voltage probe have been employed--the direct-loop or "D-loop", and the inner voltage divider. The former is made with an insulated thin wire passing through both the electrodes in such a way that it encircles all the flux linked within the chamber, but of course records no resistive drop (Fig. 14a). The latter consists of an insulated brass rod, 1.5 mm in diameter, passing through one of the electrodes, and touching the other as shown in Fig. 14b. The insulation employed is teflon rather than glass for better resistance to thermal shock. In this device, the voltage is measured between the divider tip and the electrode A. As shown in Fig. 14b, the circuit is closed along the marked path, hence no magnetic flux is enclosed and, consequently, the inner divider measures only the resistive component of the overall voltage across the chamber. Typical responses of these devices are shown in Fig. 15 a, b, and Fig. 18.

If we call V_1 and V_2 the voltage records of the

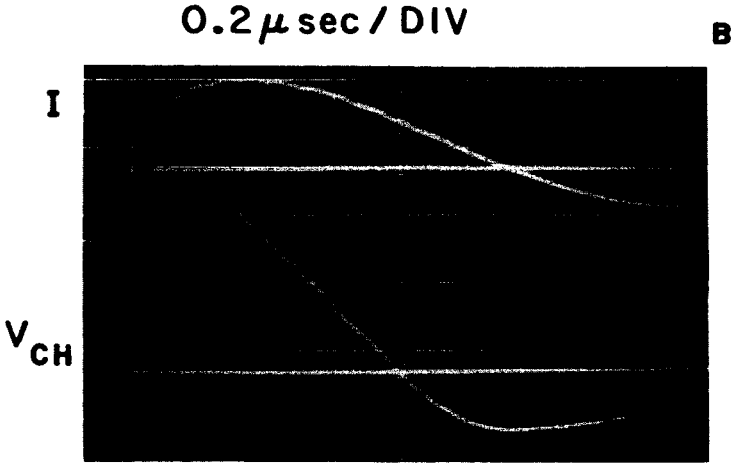

a) COMPARISON OF VOLTAGE V_{CH} & CURRENT I

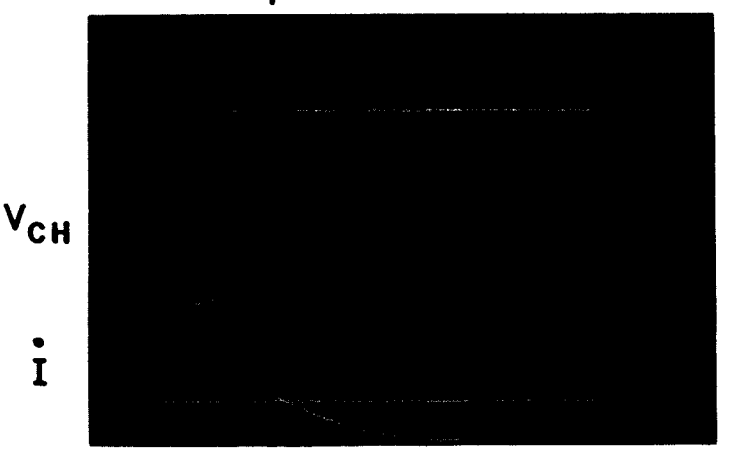

b) COMPARISON OF VOLTAGE V_{CH} & CURRENT DERIVATIVE $\dot{I}$

OVERALL VOLTAGE AND CURRENT OF PINCH DISCHARGE IN 100 μ ARGON

AP25-0113-66

FIGURE 13

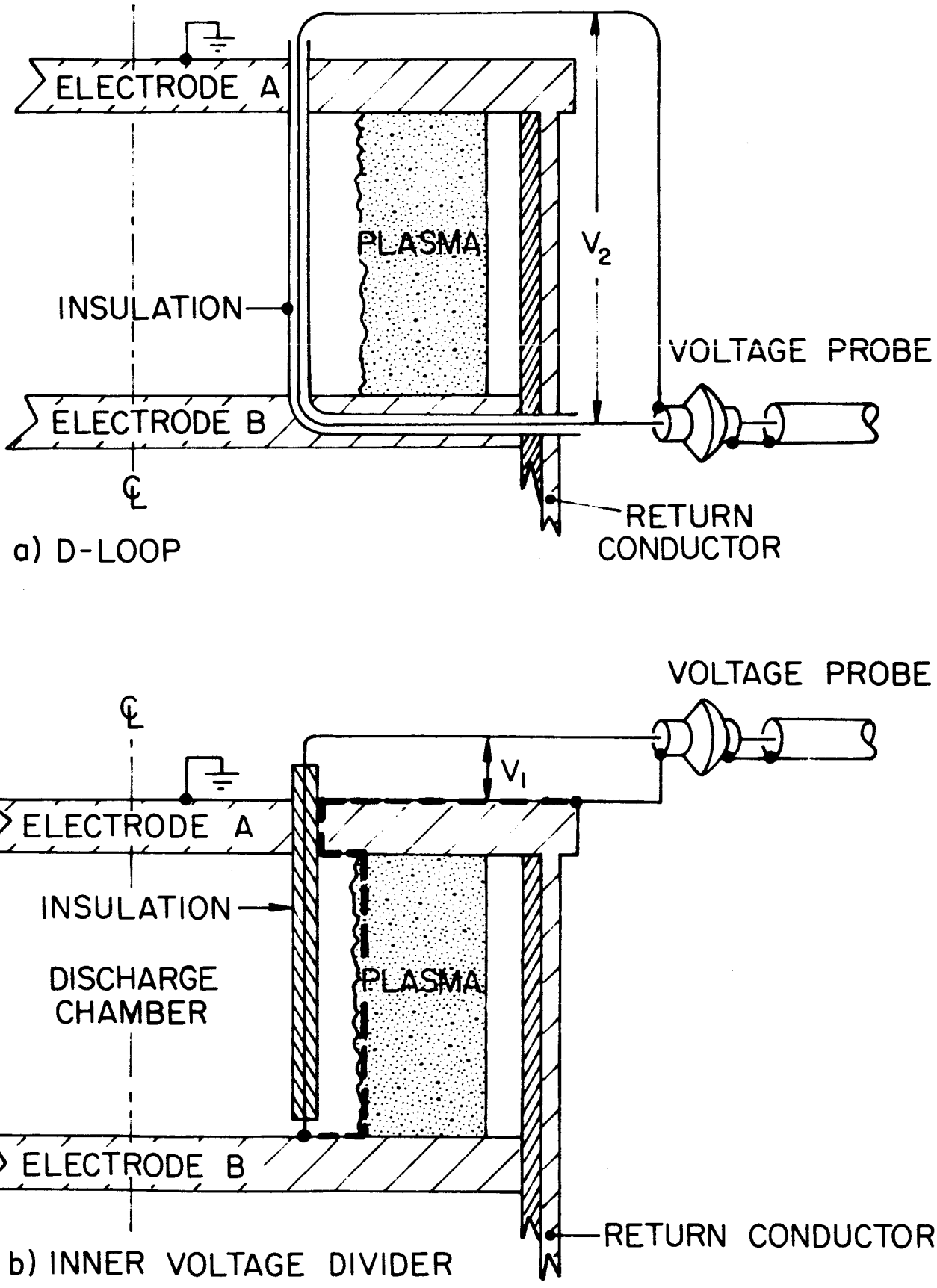

AP25-4172-66

VOLTAGE PROBES

FIGURE 14

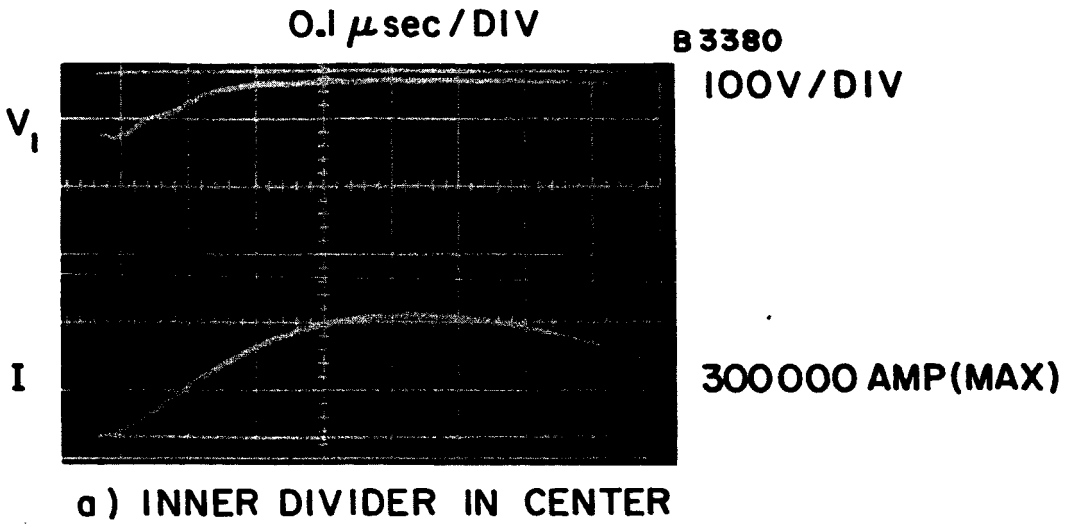

a) INNER DIVIDER IN CENTER

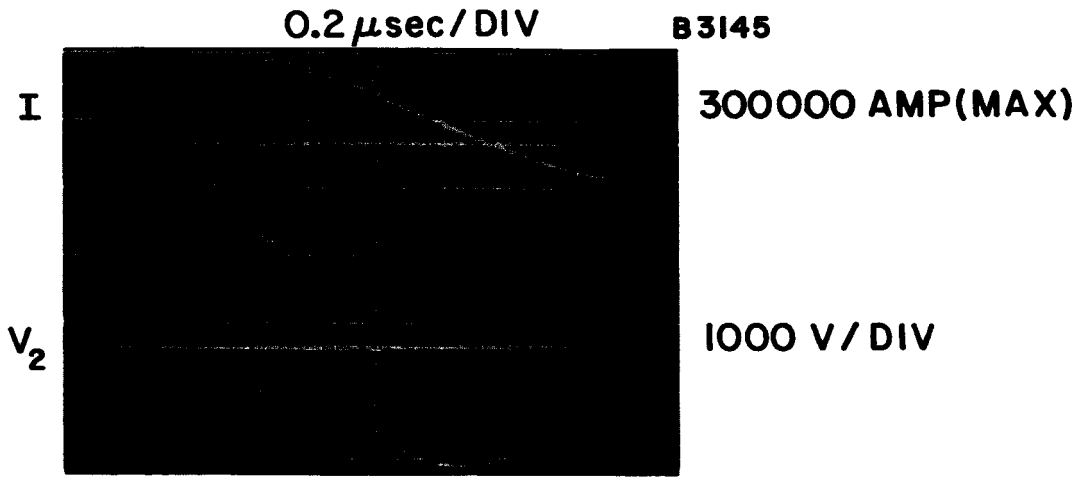

b) D - LOOP AT $R/R_0 = 0.48$

VOLTAGE MEASUREMENTS IN 100 μ ARGON DISCHARGE

APS5-P608-66

FIGURE 15

inner divider and of the D-loop, respectively, it follows that

$$V_{ch} = V_1 + V_2 \tag{22}$$

where,

$$V_1 = R_p I \tag{23}$$

and,

$$V_2 = \frac{d\phi_p}{dt} + \frac{d\phi_{in}}{dt} \tag{24}$$

It might seem that measurement of V_1 is redundant since measurement of V_{ch} and V_2 should suffice to determine it. However, V_{ch} and V_2 are of the same order of magnitude, in the kilovolt range, whereas V_1 is quite small except during discharge initiation. Hence considerable error may result from a subtraction process.

The inner divider measurements seem particularly useful during the initiation phase, and several records have been taken at various radial positions, R/R_o = .85, .66, .48, and 0. Typical responses are shown in Fig. 16. These may be explained as follows. After the breakdown, the current starts rising, but the plasma resistance decreases more rapidly, so that the inner voltage V_1 recedes to the low value $R_p I$; when the current sheet passes by the divider location, the device then ceases to be an "inner divider," but now responds to the enclosed flux variation. In the special case where the inner divider is right at the wall, the circuit will enclose all the magnetic flux, except that within the insulator. In this way it is possible to obtain only the flux variation within the plasma. A typical record is shown in Fig. 16, for $R/R_o = 0.95$. Note that excluding the $L_{in} \frac{dI}{dr}$ term from the voltage trace yields a different phase and less steep first half cycle than the V_2 records.

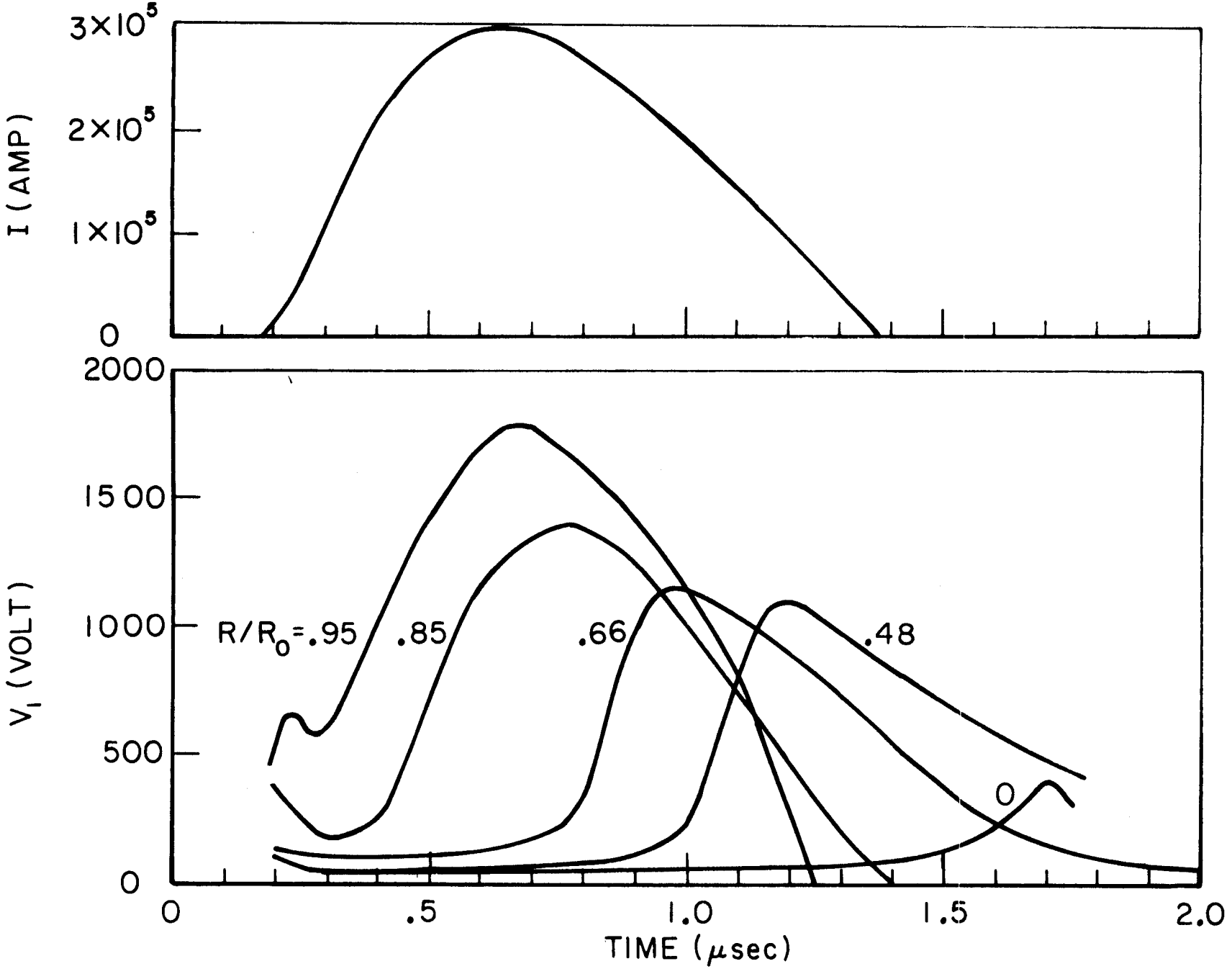

FIGURE 16

RESPONSE OF INNER VOLTAGE DIVIDER AT VARIOUS RADIAL POSITIONS

On the basis of measurements such as these it is now possible to conclude that the resistive component of the voltage across the current sheet does not exceed 30 V while the overall voltage reaches about 2.5 KV at the maximum. For a peak discharge current of some 3 x 10^5 amps, a plasma resistance of the order of 10^{-4} ohms is thus indicated. The plasma inductance is of the order of 10^{-8} henry and its derivative with respect to time 10^{-2} henry/sec. These experimental results are in good agreement with the snowplow theoretical calculations, for at least the first microsecond of the records where the second current sheet has not yet reached an appreciable strength.

Study of the breakdown mechanism was begun by experimental determination of the Paschen curve for argon in the same apparatus described above. The curve was traced out by connecting the capacitor bank directly to the two electrodes of the chamber, and then slowly increasing the voltage until breakdown occurred at the set pressure. The range of pressure covered was from 22 to 1700 μ, corresponding to a pressure x gap spacing (pd) range from 110 to 8500 μ-cm. The measured Paschen curve is shown in Fig. 17.

A second series of breakdown data was collected using the chamber in its normal circuit, with a 1000 ohm resistor in parallel, and recording the electrode potential on a very rapid time base (0.1 μsec/cm) using the inner voltage divider. This divider was placed in the center of the chamber to avoid flux linkage. A typical response is shown in Fig. 18a; and suggests the following qualitative explanation. When the switch is closed, the voltage rises to the sparking value in about 0.04 μsec, at which time the chamber breaks down. Although the current also increases rapidly from this time, the conductivity of the gas increases even more rapidly, and the gap voltage falls steadily. The magnitude of the voltage peak is found to be independent of the bank voltage, but dependent on the chamber pressure. The results

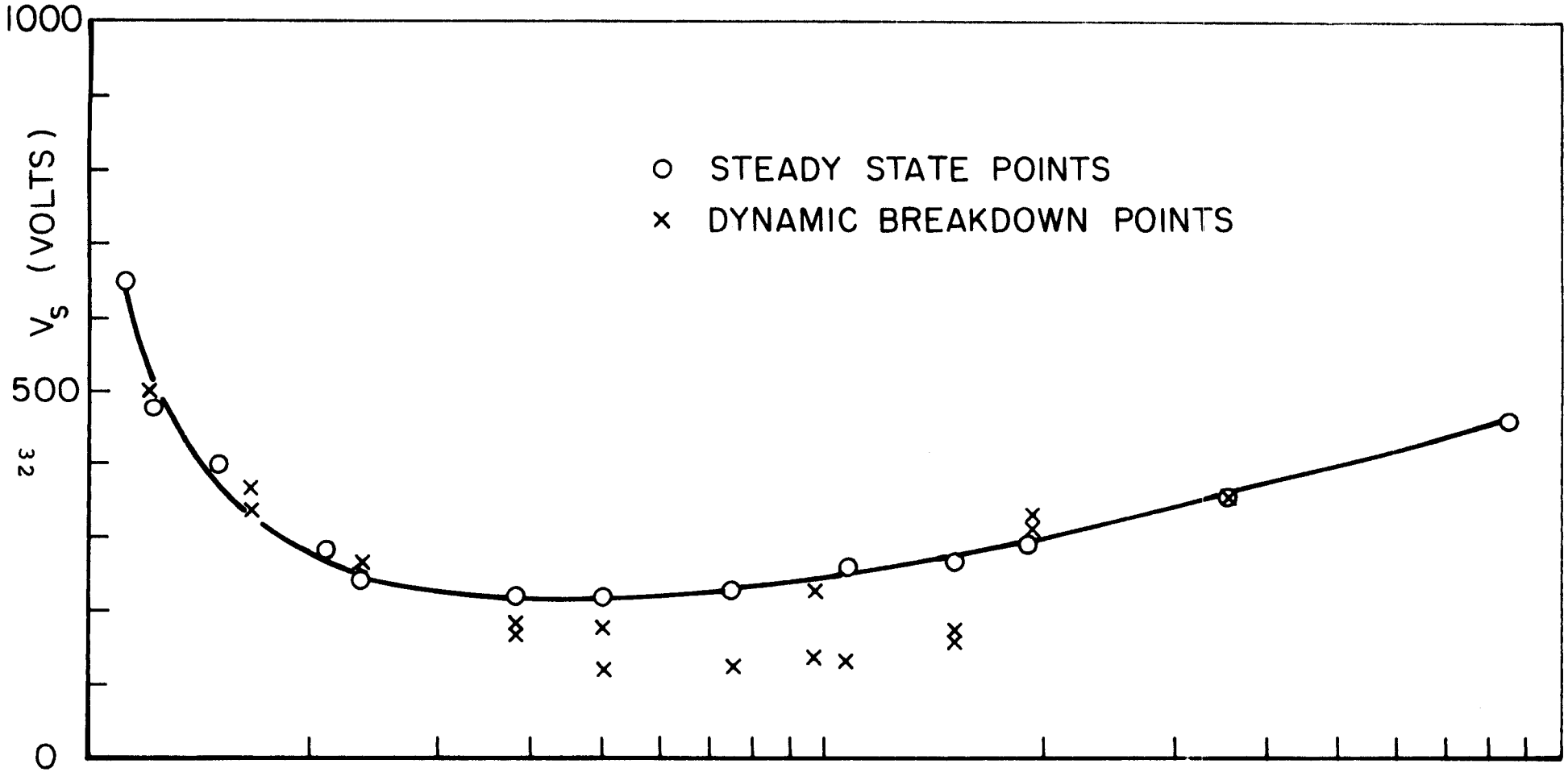

FIGURE 17

PASCHEN CURVE FOR ARGON

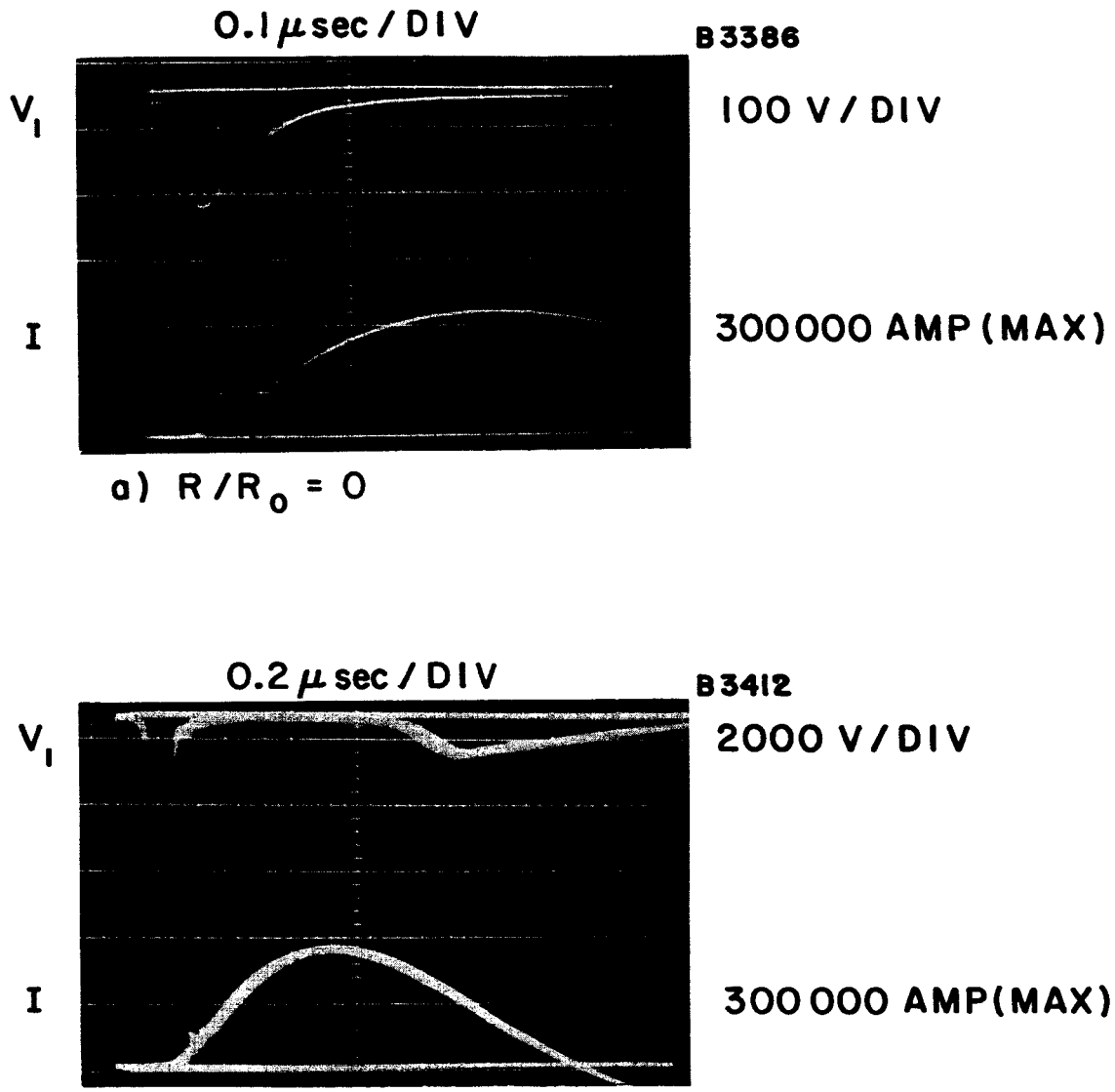

RESPONSE OF INNER VOLTAGE DIVIDER

APS-PSTD-66

FIGURE 18

obtained varying the pressure are also shown in Fig. 17 indicated as dynamic breakdown points.

After this series of experiments, the electrode surfaces were polished somewhat, and the sequence repeated. In this case, order of magnitude higher voltage peaks were obtained--of the order of 7-8 KV (Fig. 18b). These peaks were also quite reproducible, and were confirmed by overall voltage measurements, (Fig. 19a) but were not observed with the D-loop (Fig. 19b) thus excluding any flux change dependence.

A possible explanation of this strong dependence of breakdown voltage on surface condition is that the time required by the gas to break down is increased by clean electrodes. Over this longer time, the current would continue to rise through the parallel external resistor, and the voltage across the electrodes would increase correspondingly. To check this hypothesis, several measurements were made with various smaller values of the external resistor, and with some inductance in series with it, to slow down the current rise and hence to lower the voltage peak. No substantial variation in maximum voltage attained were found in any of these cases.

It thus seems that the electrode surfaces control the transient breakdown voltage, per se. To follow this point, a series of measurements were taken with a highly polished pair of electrodes. In this case the gap voltage was found to reach the full 10 KV bank voltage, and to remain there for a finite time interval, primarily dependent on gas pressure (Fig. 20a-d, and 21).

Further studies on the effect of electrode surfaces on breakdown transients are in progress in the hope of identifying the role of electrode material in the initiation process.

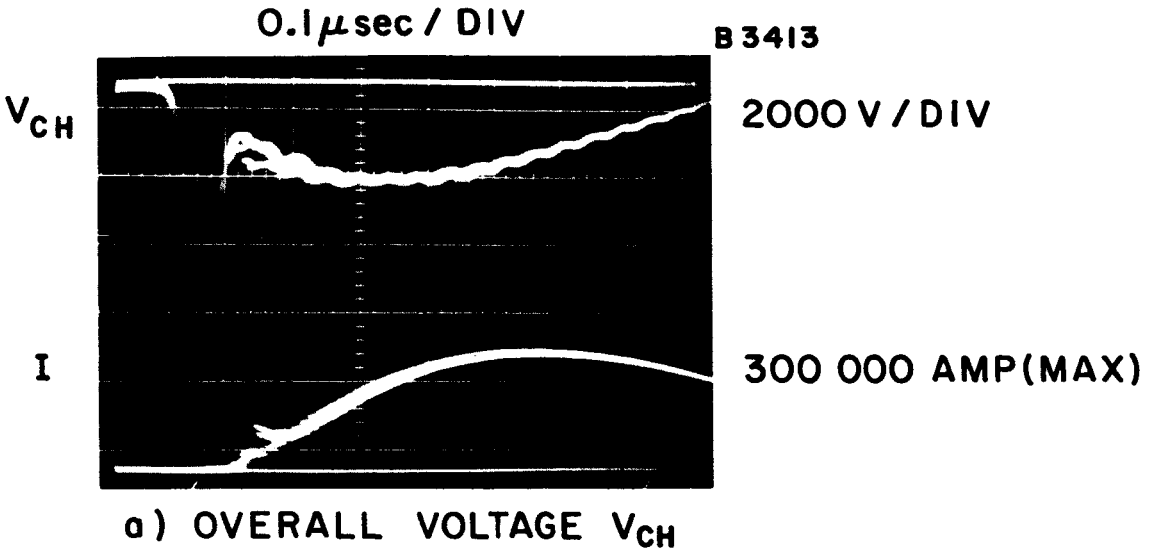

a) OVERALL VOLTAGE V_{CH}

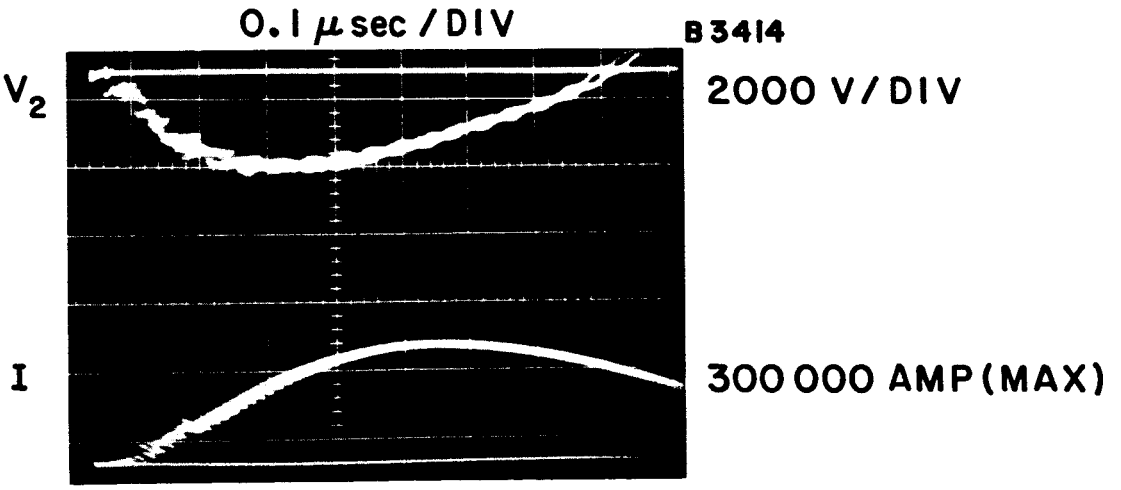

b) D-LOOP VOLTAGE V_2

AD2S-PSBB-76

VOLTAGE MEASUREMENTS IN ARGON DISCHARGE

FIGURE 19

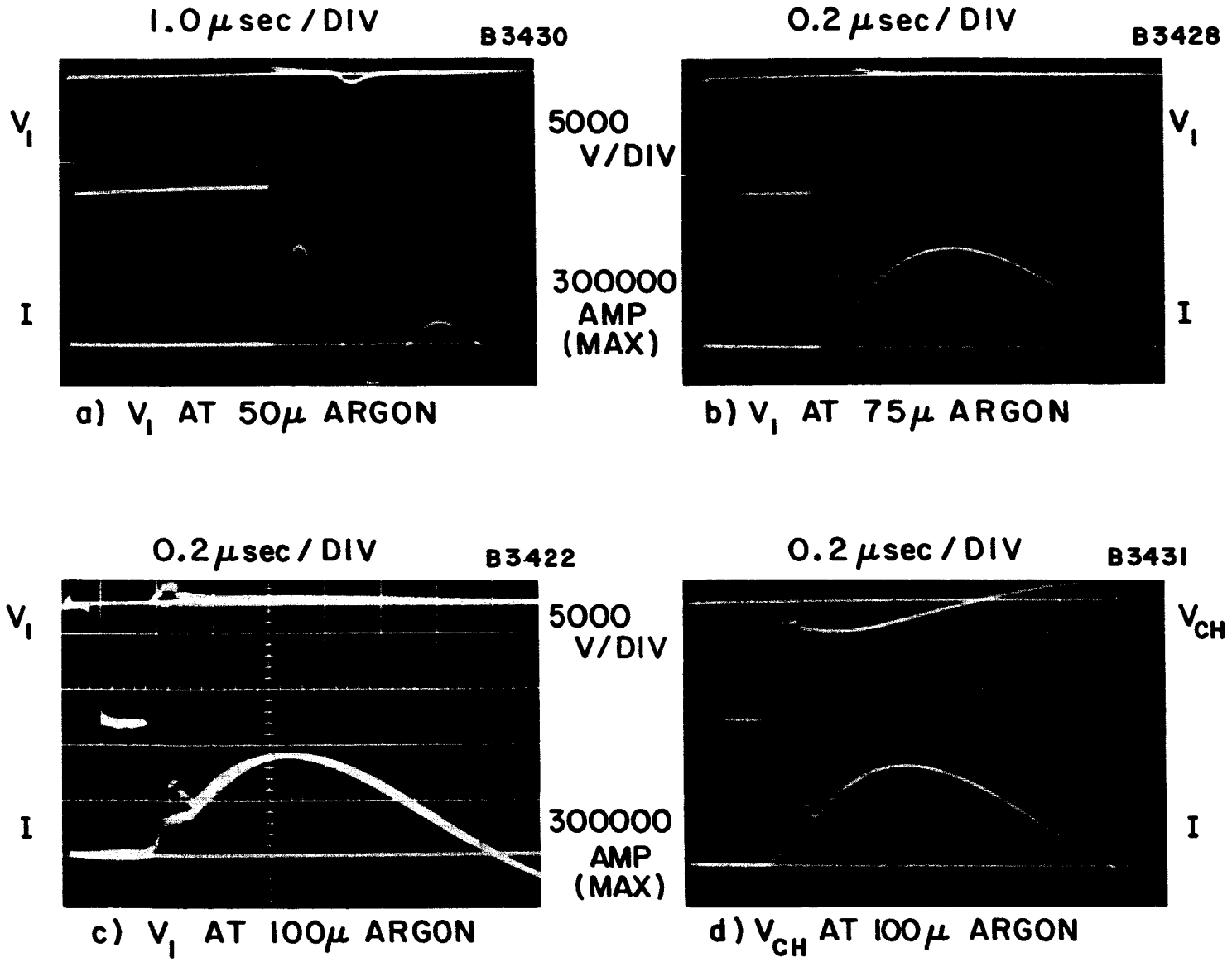

VOLTAGE RESPONSES AT BREAKDOWN

AD25-P578-66

FIGURE 20

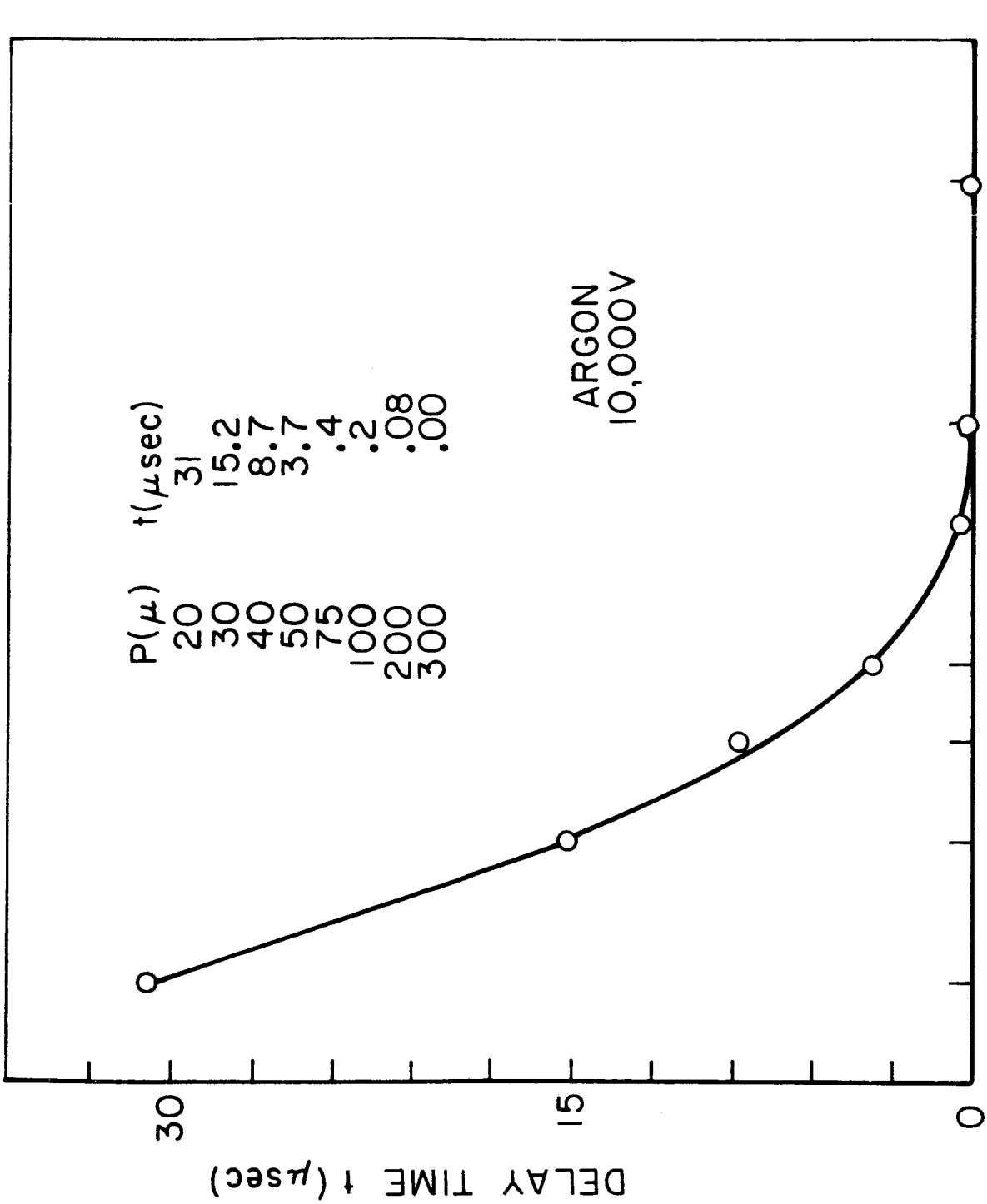

DEPENDENCE OF BREAKDOWN DELAY TIME ON PRESSURE

FIGURE 21

AP25-4175-66

V. GAS LASER INTERFEROMETER FOR ELECTRON DENSITY MEASUREMENTS (Cooke)

It is desired to develop a laser interferometer capable of providing measurement of the electron density profiles which develop during typical pulsed plasma acceleration processes. Data of this sort, particularly in the region of high density, highly ionized current sheets, could then be correlated with previous experimental results of other measureables and with analytical models. This measurement has resisted several other diagnostic techniques especially in the more vigorous discharges,[I-39] including our own millimeter wave reflection probe. In optical interferometry laser light sources are preferred because of their high intensity, coherence, monochromaticity, and unidirectionality.[II-1]

All interferometric methods of electron density measurement are based on the functional dependence of the refractive index of a plasma on its free-electron density. Recently Ashby and Jephcott described an interferometric method which, in addition to using a laser light source, relied upon a self-modulation of the laser cavity by its own reflected light to simplify the optical apparatus.[II-2] Several papers on this subject have been written since, and have encouraged this technique. However, these papers present conflicting accounts of the time resolution obtainable, by this technique, i.e. of the relaxation time of the self-modulation process.

This interferometer cavity will support resonance when the optical path in the cavity is a multiple of the laser radiation wavelength, the optical path being defined as the integral of the cavity refractive index over the physical length traversed, i.e., from the laser mirror to the external mirror and back. As the optical path varies, the light intensity in the interferometer cavity will change

in a periodic manner, each period being a complete cycle of light intensity called an interferometric "fringe." Because the light intensity in the external cavity strongly affects the lasing process, corresponding changes (fringes) in laser intensity are observed from the opposite end of the laser (Fig. 22a). Therefore, when a chamber of ionized gas is placed in the external cavity, changing electron density, because of its affect on refractive index, can be monitored by means of the fringes seen in the lasing intensity. In our proposed application, a typical discharge in 100 μ Argon is expected to sweep a 0.5 cm. thick current sheet with an electron density of 10^{17} cm^{-3} past the probing laser beam in 10^{-7} seconds, thus producing interference fringes at a rate of up to 10^{8} fringes per second for laser radiation in the visible or near infrared. Several investigators report that the maximum frequency response of the Ashby-Jephcott interferometer is less than 10^{6} fringes per second.[II-2,3,4 and 5]

Our first studies, therefore, consisted of measuring the response time of our version of the interferometer, using a moveable external mirror to vary the optical path. A Spectra Physics Model 130 He-Ne gas laser emitting red light at a wavelength of 6328 angstroms was directed at a rotating streak camera mirror (Fig. 22b). When the fringing frequency approached 10^{6}/sec, the suspected modulation degradation was verified (Fig. 23).

It appears then that the fringing rate obtained with the Ashby-Jephcott interferometer is two orders of magnitude below that required for our application. Fortunately, it seems possible to improve the response of this device up to the required 10^{8} fringes per second, by a relatively trivial change in the optical arrangement (Fig. 22c). Reasons for the large variance in obtainable fringing rates between the

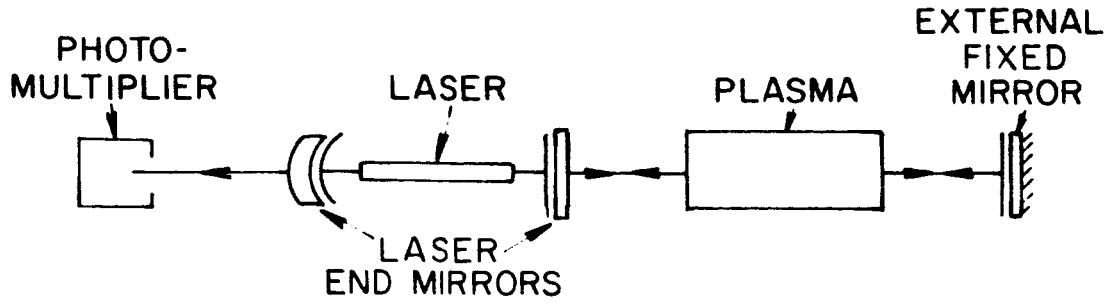

a) ASHBY-JEPHCOTT ARRANGEMENT

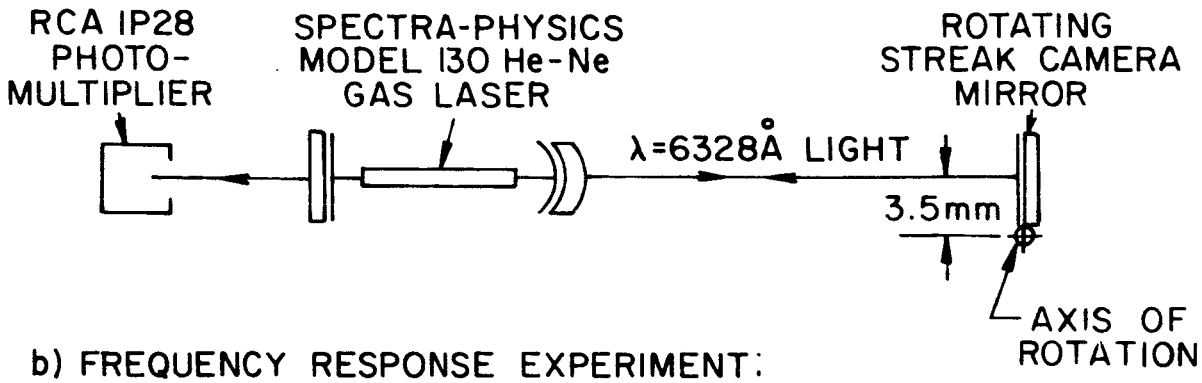

b) FREQUENCY RESPONSE EXPERIMENT:
ASHBY-JEPHCOTT ARRANGEMENT

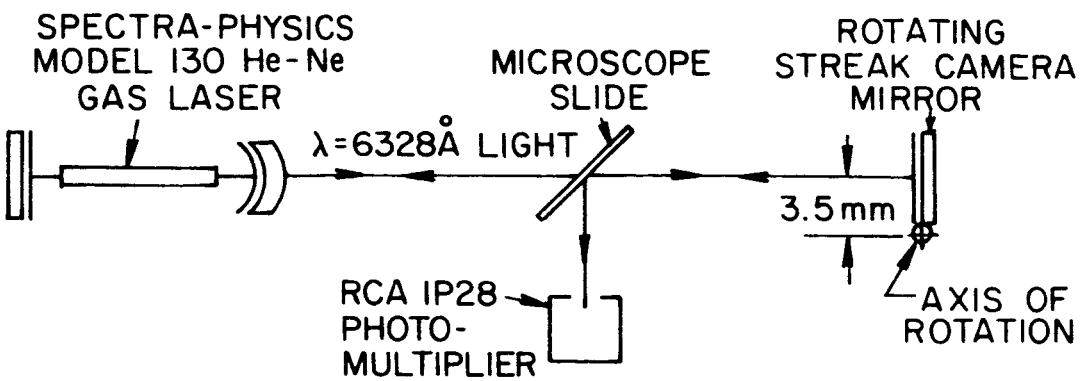

c) FREQUENCY RESPONSE EXPERIMENT:
MODIFIED ARRANGEMENT

AP25-4174-66

THE LASER INTERFEROMETER

FIGURE 22

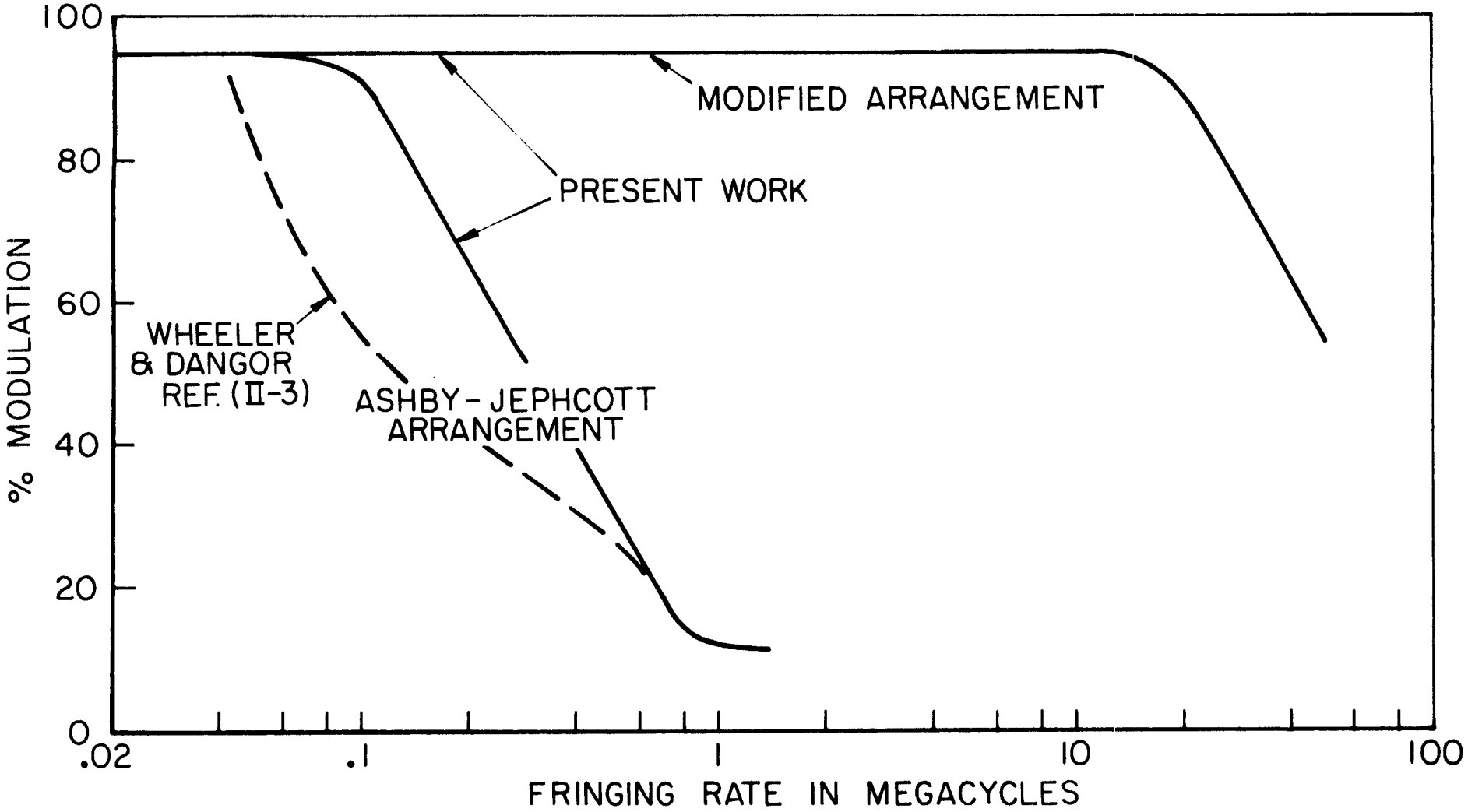

FIGURE 23

MEASURED FREQUENCY RESPONSE OF LASER INTERFEROMETERS

two detection sites are explained in the literature.[II-4,5] Because of the falloff in high frequency response of the available oscilloscope, modulation results were not obtained beyond 50 MC (see Fig. 23). Sample oscillographs with fringing rates from 100 KC to 50 MC are shown in Fig. 24. The lower traces show the modulation of the light, and the straight line in the middle of each oscillogram is the zero light signal. The upper traces monitor the speed of revolution of the rotating mirror and are used to compare the actual and calculated fringing rates, which always agree within ten percent. Since the laser beam falls on the streak camera mirror only 3.5 millimeters from its axis of rotation (measured perpendicularly to the beam), the mirror reflects the light back along the incident beam for only a very short travel of the mirror. Based on the measured divergence of the beam, the total number of fringes should be about seven, which is seen to be the case in Fig. 24, with the modulation level decreasing on either side of dead center due to the smaller amount of light in the reflected beam being reflected back along the incident beam.

With these preliminary experiments the applicability of the laser as a diagnostic tool for obtaining detailed time and space resolution of free electron density in the dense, highly ionized current sheet has been verified. Once the plasma environment is shown not to interfere with these measurements at a particular laser wavelength, the interferometer will be installed on a pinch machine.

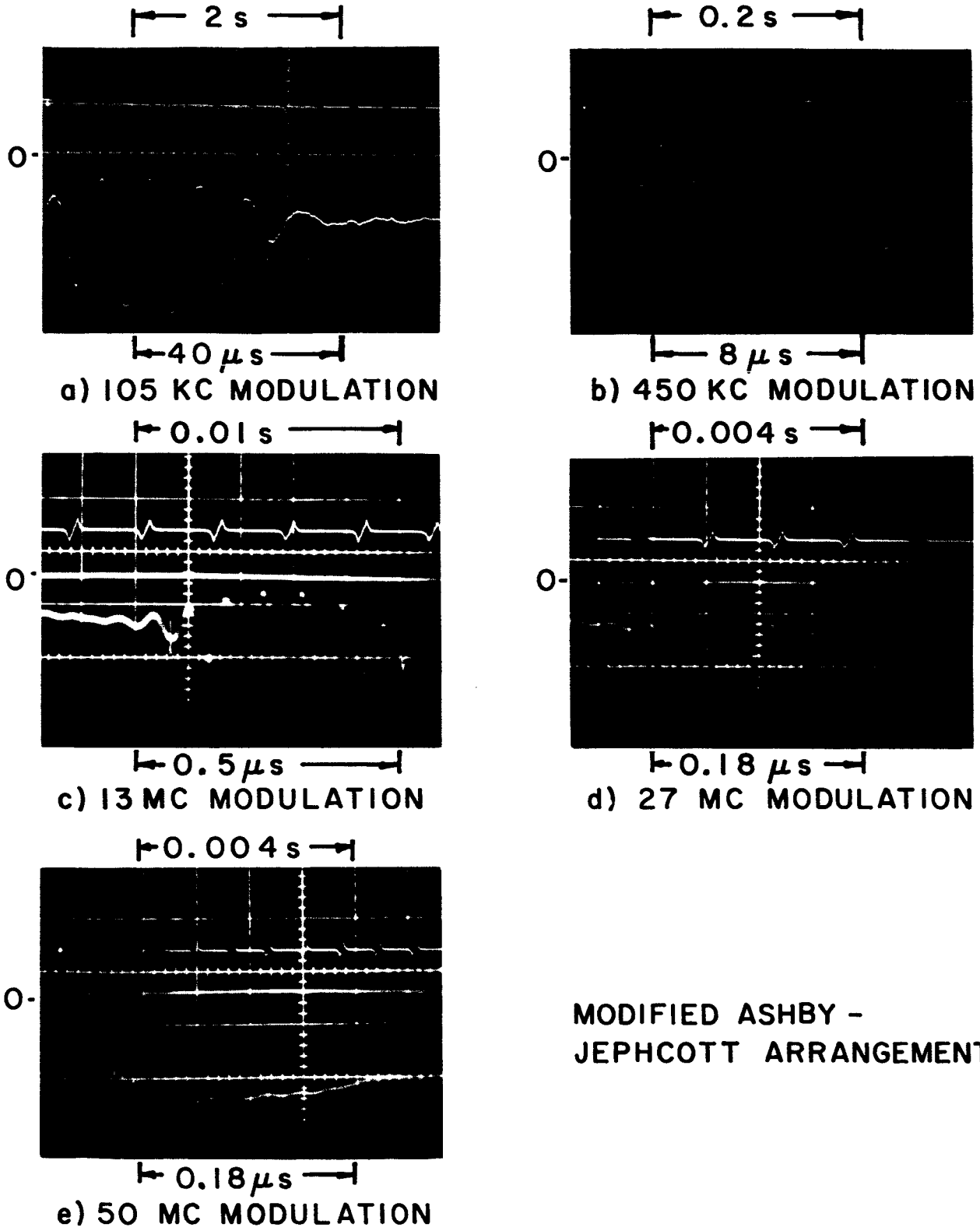

MODIFIED ASHBY - JEPHCOTT ARRANGEMENT

AD-S-P638-66

MODULATION OF LIGHT IN MODIFIED INTERFEROMETER ARRANGEMENT

FIGURE 24

VI. REFINEMENTS IN MICROWAVE PROBE TECHNIQUES (Ellis)

In the last report,[I-32] the basic elements of a theory relating measurements of the complex reflection coefficient $R = |R| e^{i\varphi_r}$ of a lossy, inhomogeneous plasma to the fundamental plasma parameters such as number density, $\bar{n}/\bar{n}_{crit}$, and collision frequency, ν_c/ω was presented. During this reporting period, the techniques of measuring $|R|$ and φ_r in the laboratory have been improved. These measurements have proved to involve some rather subtle points.

Phase measurements can only be made indirectly, by employing the interferometer principle. The microwave interferometer previously described [I-32] responds to the net electric field at the detector, which field may be expressed as the vector sum of a unit reference signal and the complex reflection coefficient in the normalized form

$$E_{net} = \frac{S \pm}{2} = \frac{[1 + |R|^2 \pm 2|R|\cos\varphi_r]^{1/2}}{2} \qquad (25)$$

The choice of the + or - sign in Eq. 25 is in the hands of the experimenter, this choice determining whether the bridge yields a null or anti-null when incorporating the reflected signal; viz, whether the signals add or subtract. For convenience we will refer to use of the + sign as "mode 1" operation, and use of the - sign as "mode 2" operation. Both modes have their uses.

Operation of these modes with a square law detector is shown in Fig. 25 and Fig. 26, for reflections calculated from a semi-infinite plasma slab using a previously described model.[I-32] Figures 27a and 27b show the actual response of the interferometer to a discharge in 30 μ of Argon. The greater cusp heights of mode 1 operation, in Fig. 25 and 27a,

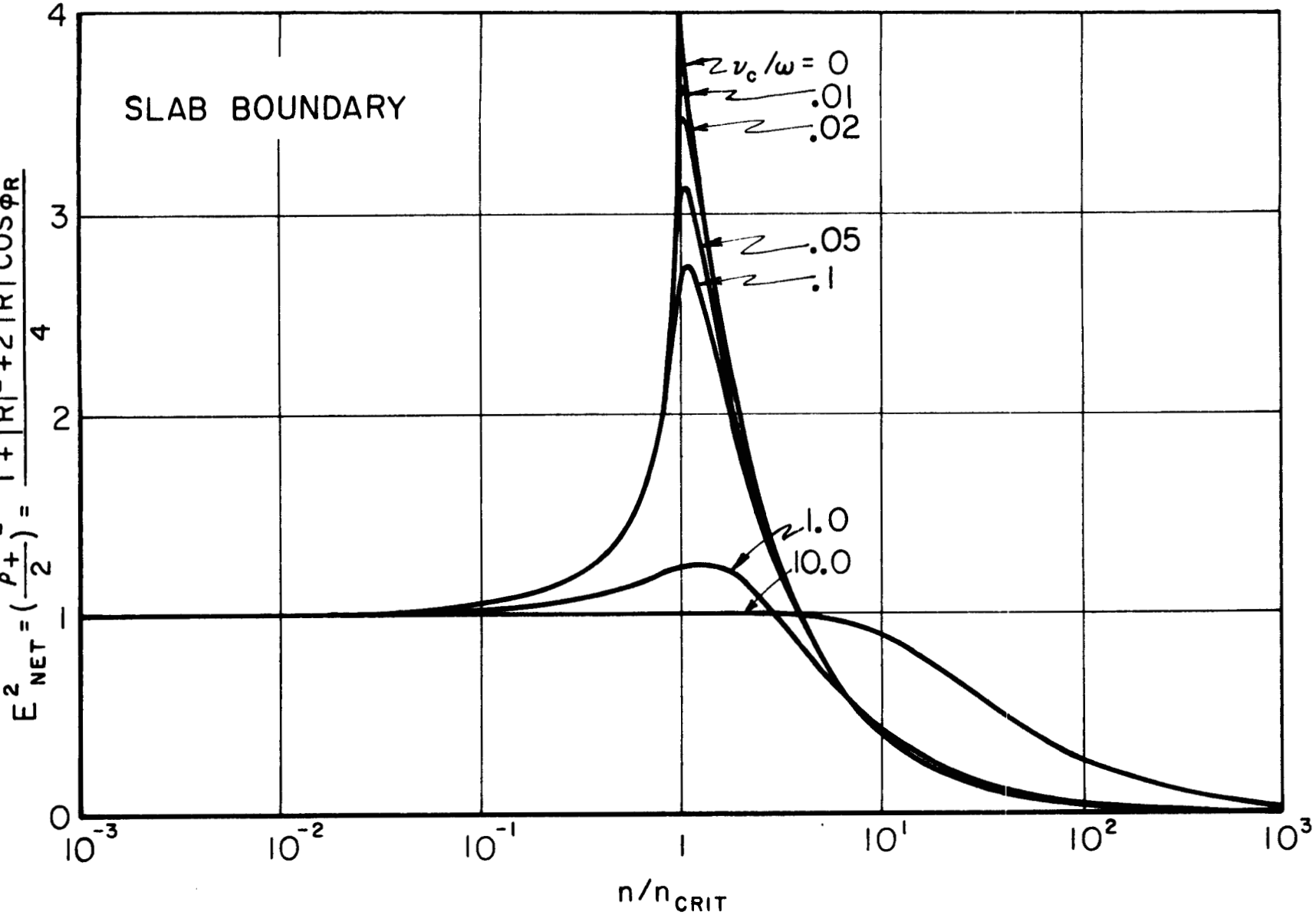

FIGURE 25

COMPUTED INTERFEROMETER RESPONSE AS A FUNCTION OF ELECTRON DENSITY AT SLAB BOUNDARY, MODE I OPERATION

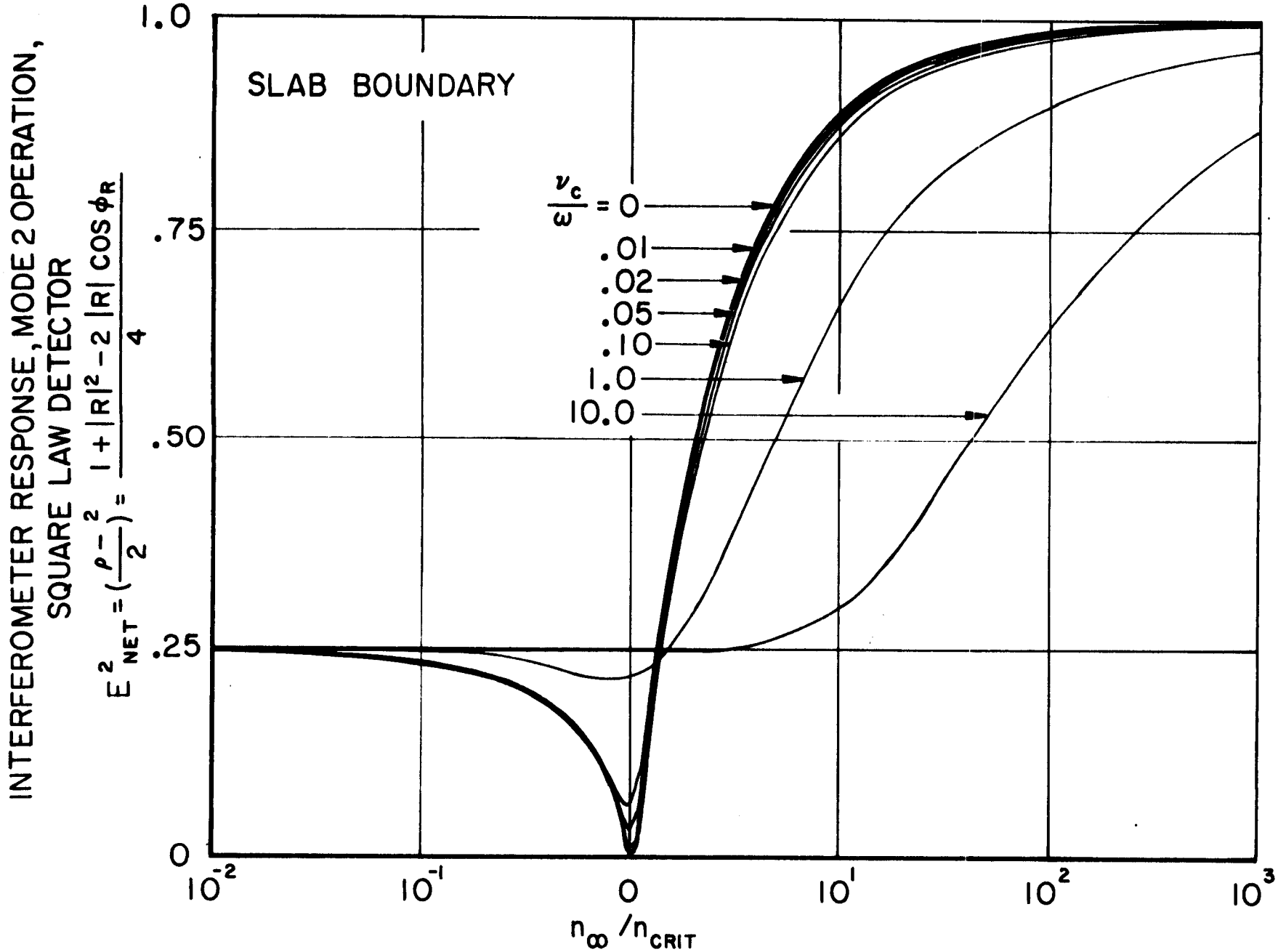

COMPUTED INTERFEROMETER RESPONSE AS A FUNCTION OF ELECTRON DENSITY AT SLAB BOUNDARY, MODE 2 OPERATION

FIGURE 26

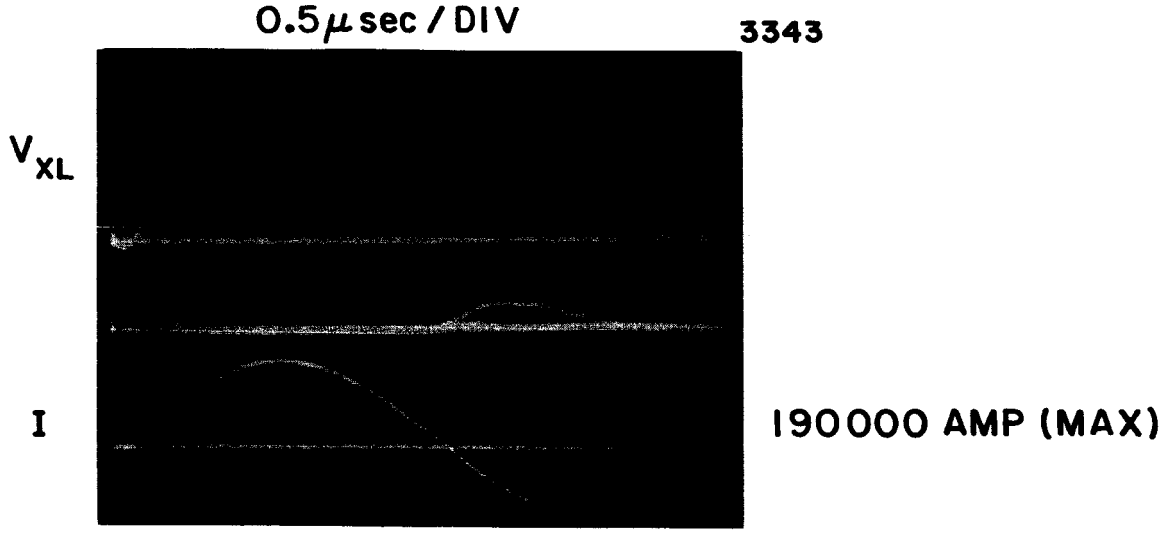

a) MODE "1" OPERATION
(DOUBLE OVERLAY)

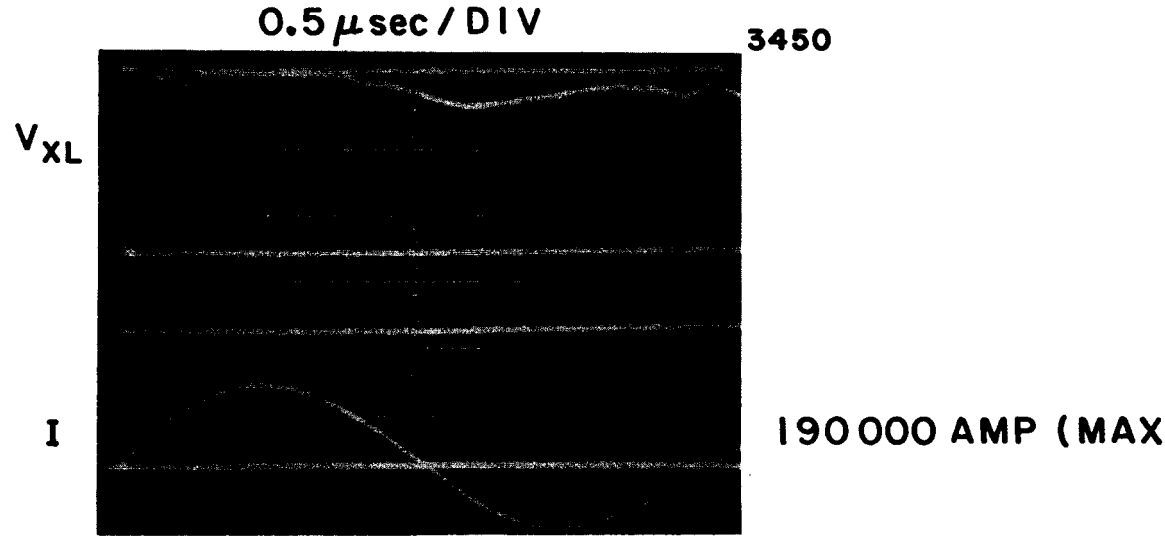

b) MODE "2" OPERATION

MEASURED RESPONSE, V_{XL}, OF MICROWAVE INTERFEROMETER TO DISCHARGE IN 30μ ARGON, AT $R/R_0 = 0.5$, HORN FLUSH IN ANODE

FIGURE 27

clearly demonstrates its greater sensitivity to collisional damping, and hence to measurements of ν_c/ω. Figure 27a also shows the absence of the top reference line in mode 1 operation, an unavoidable feature which makes mode 1 operation in general difficult to calibrate.

Figures 28 and 29 show computed interferometer responses for the two modes from a plasma with an exponential density gradient at the boundary, $\eta(z) = \eta_\infty (1 - e^{-(2mz)/\lambda_o})$, assuming a constant collision frequency and a detector with a linear response law. These figures are simply plots of Eq. 25 based on the theory presented in the previous report.[I-32] Instead of using the quantity "m" in the exponential to identify these curves, a new parameter Z^* is employed. Z^* is defined to be the value of Z/λ_o, for a given m, which makes $\eta(z)/\eta_\infty = 1 - e^{-2mz/\lambda_o} = 0.99$. Thus the physical interpretation of Z^* is the thickness of the gradient region in units of λ_o, the free space wavelength.

A linear detector can be realized in practice by employing a forward voltage biasing circuit in conjunction with a Philco IN2792 germanium diode and a compensating circuit for the oscilloscope. The measured volt ampere characteristic, employing normalized quantities actually used for the experiments, is shown in Fig. 30. The linearity of this characteristic is evident. Its usefulness stems from the fact that mode 1 operation can now be more easily calibrated, by locating a top calibration line at twice the height of the central calibration line. This is significant because a unique determination of ramp thickness at the plasma boundary becomes possible by operating the bridge in both mode 1 and mode 2.

A close examination of Figures 28 and 29 shows that they are not symmetrical about the center line, a condition

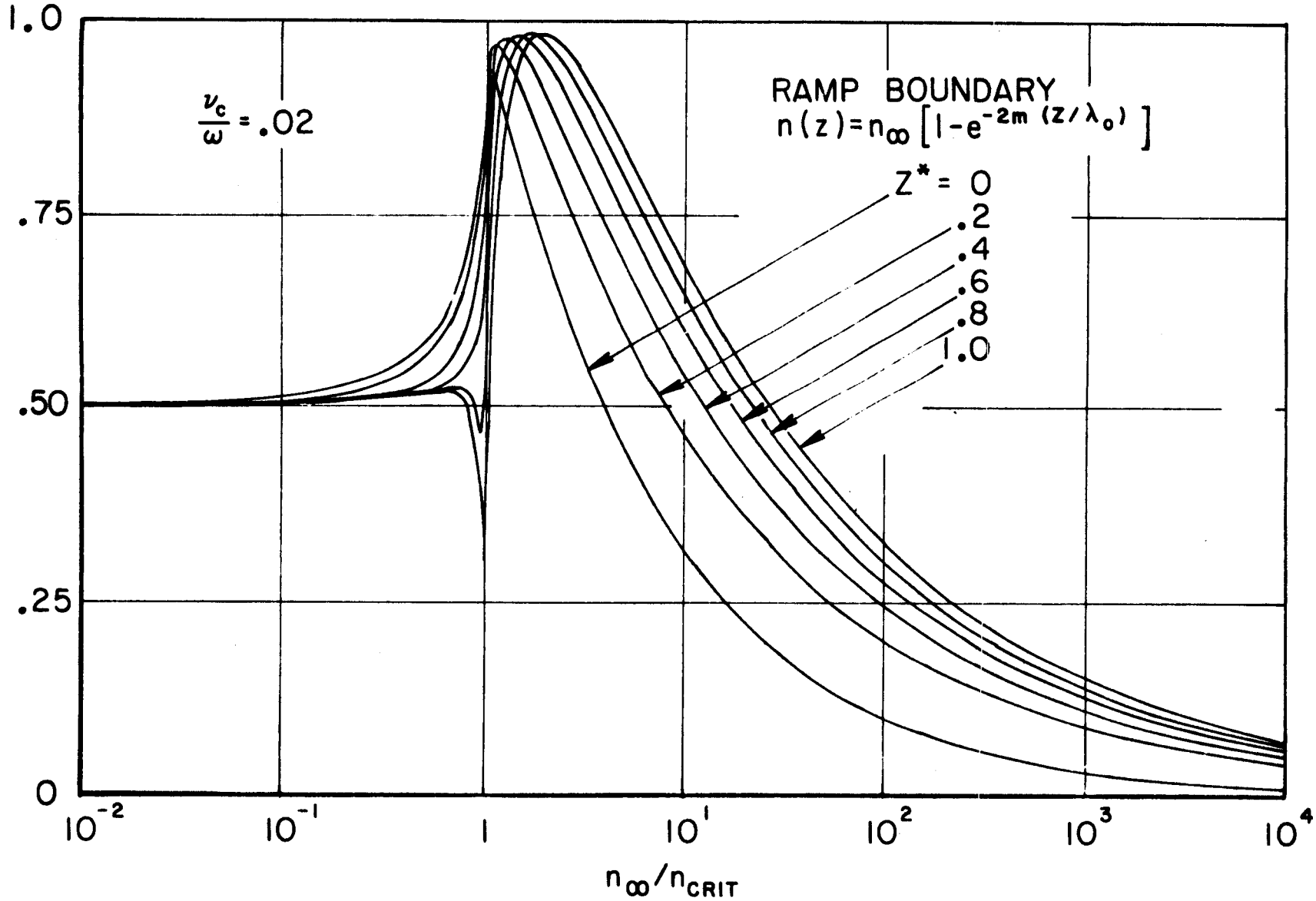

FIGURE 28

COMPUTED INTERFEROMETER RESPONSE AS A FUNCTION OF ELECTRON DENSITY WITH RAMP BOUNDARY, MODE I OPERATION

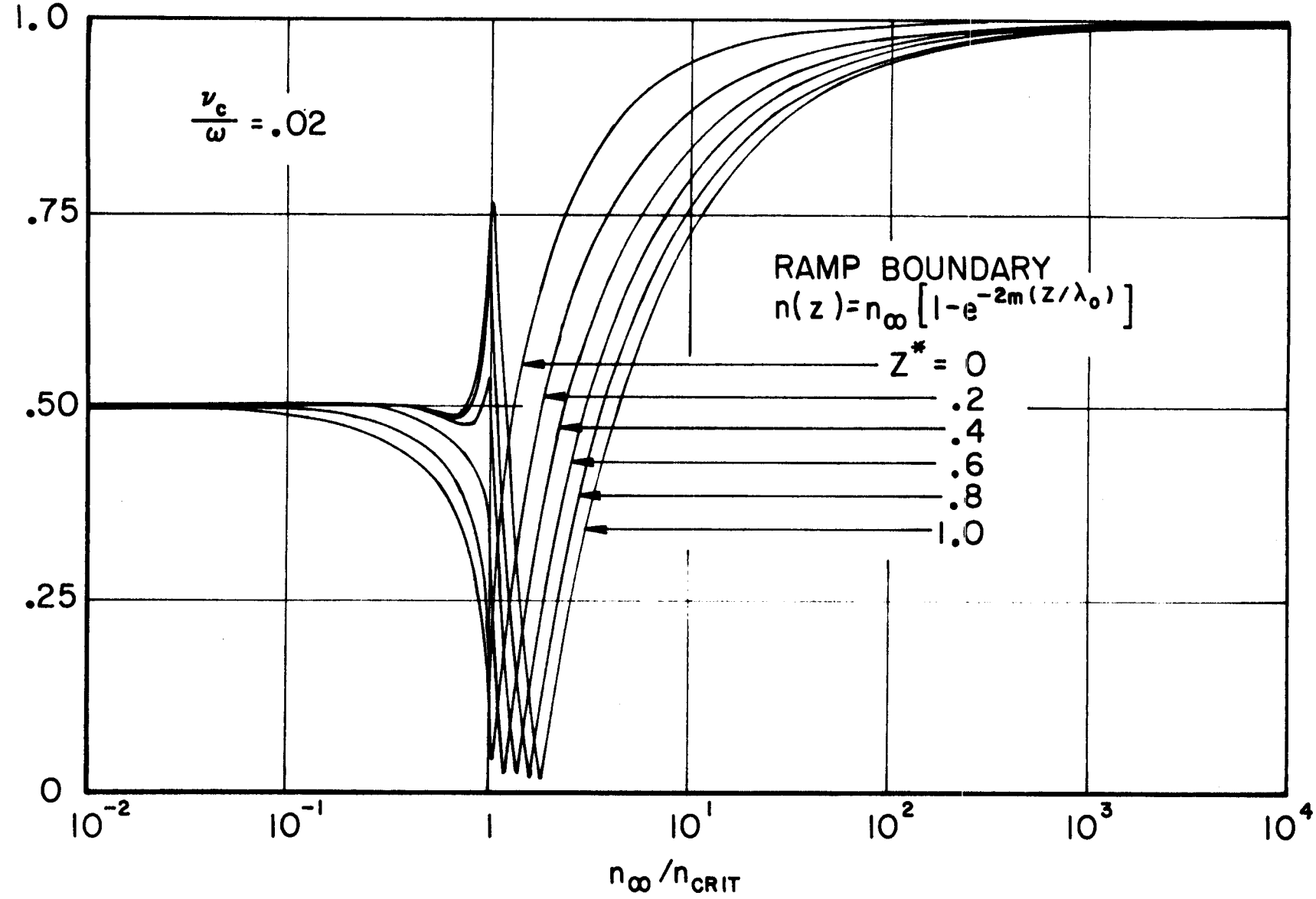

FIGURE 29

COMPUTED INTERFEROMETER RESPONSE AS A FUNCTION OF ELECTRON DENSITY WITH RAMP BOUNDARY, MODE 2 OPERATION

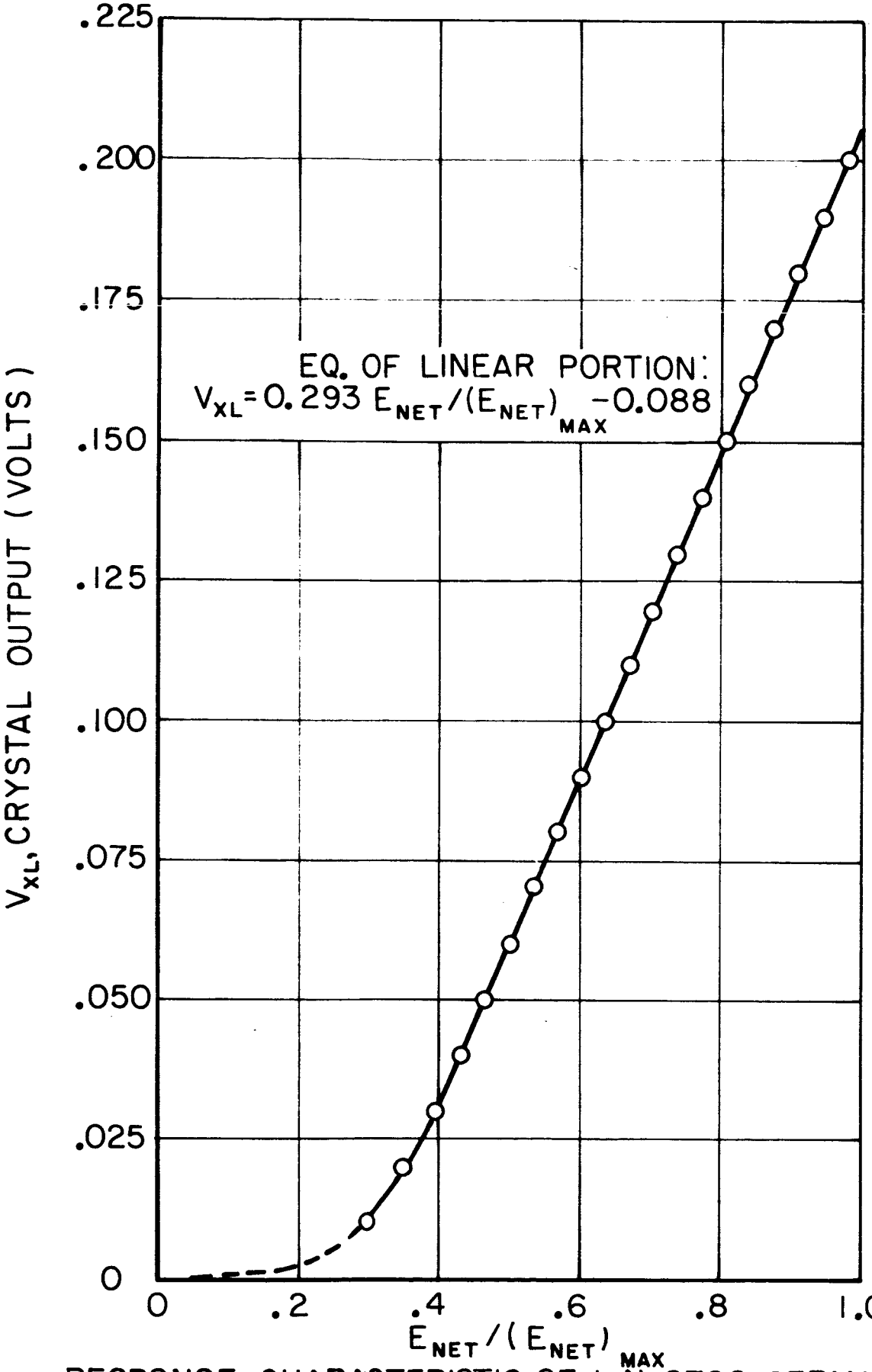

RESPONSE CHARACTERISTIC OF 1 N 2792 GERMANIUM DIODE DETECTOR

FIGURE 30

AP25-4180-66

arising from the square root function in Eq. 25. The curves of Fig. 28 are much more closely bunched at high densities than are those of mode 2 in Fig. 29. Simultaneous measurement of $\rho/2$ in each mode, with linear detectors, determines a unique value of the ramp parameter which can be read off directly from these curves, and used to yield values of electron density vs. time. Collision frequencies can still be determined, from other computed sets of these curves, because the ramp thickness, Z^*, does not appreciably affect cusp height.

The model used for these computed curves assumes a plane wave incident on the plasma boundary.[I-32] Departure of the experimental situation from this presumption causes no trouble so long as the incident microwave energy is, or can be, totally reflected by the plasma. Due to the roughly spherical nature of the emerging wavefront diffracting out of the horn mouth, there is a tendency for some energy to "leak" transversely down the boundary layer, in violation of one-dimensional assumptions; this would cause $|R|_{max} < 1$, and appropriate corrections would have to be applied to the data. Thus it is necessary to measure $|R|$ simultaneously whenever $\rho/2$ measurements are made with the interferometer. These measurements together will determine the complex reflection coefficient uniquely.

$|R|$ measurements cannot, by definition, be dependent on the phase of the reflected signal. This condition is usually assumed to be satisfied if a null is first set at the detector, but it has been found that such balancing methods are not sufficient to guarantee accurate measurements of $|R|$. To check phase-sensitivity, a movable metallic reflector placed in the waveguide at the equivalent of the horn position can be oscillated back and forth. The ideal result, $|R| = 1$ with no oscillations, was never observed to

occur. Oscillations were always present, apparently due to the altered effective termination impedance appearing at the waveguide end when reflections were introduced. The situation is not unlike the mechanical concepts of static and dynamic balancing. The dynamic balance, as it were, was accomplished with a reflection bridge, which could be balanced to give $R = 1$ with no oscillations from a metallic plunger by introducing a bucking signal of carefully chosen amplitude and phase to cancel the spurious oscillations. The procedure is tedious and involved, but the reflection measurements which have been made using this approach are considerably more accurate than those previously obtained.

The detailed results of microwave measurements on the dynamical plasma events in closed chamber discharges are currently being reduced, and will be presented in full in a forthcoming Ph.D. thesis to be completed during the coming 6-month period.

VII. HIGH-PERFORMANCE CAPACITOR DEVELOPMENT (Staff-Corson)

The program of design and construction of a series of low-inductance capacitors suitable for simple assembly into pulse line configurations has continued along the schedule outlined in the proposal.[I-27] Based on preliminary low voltage models, a full-scale 10 KV prototype was assembled and tested as an isolated unit. This capacitor, shown in Fig. 31, is 7-1/4(H) x 10"(W) x 7-5/8"(L) in dimension, weighs 26-1/2 lbs., and was found to have a capacitance of 7 μfd, and a self-resonant frequency of 1 megacycle. Following this satisfactory operation, three other identical capacitors have been assembled, and now are being tested in various connection configurations to determine the behavior of the group when assembled as a line. Presuming confirmation of the anticipated low-impedance tailored-pulse capability of this assembly, a final group of six units will be added which, along with the present four, should provide the current pulse length and magnitude desired for matched impedance acceleration studies in the 8" closed chamber discharges.

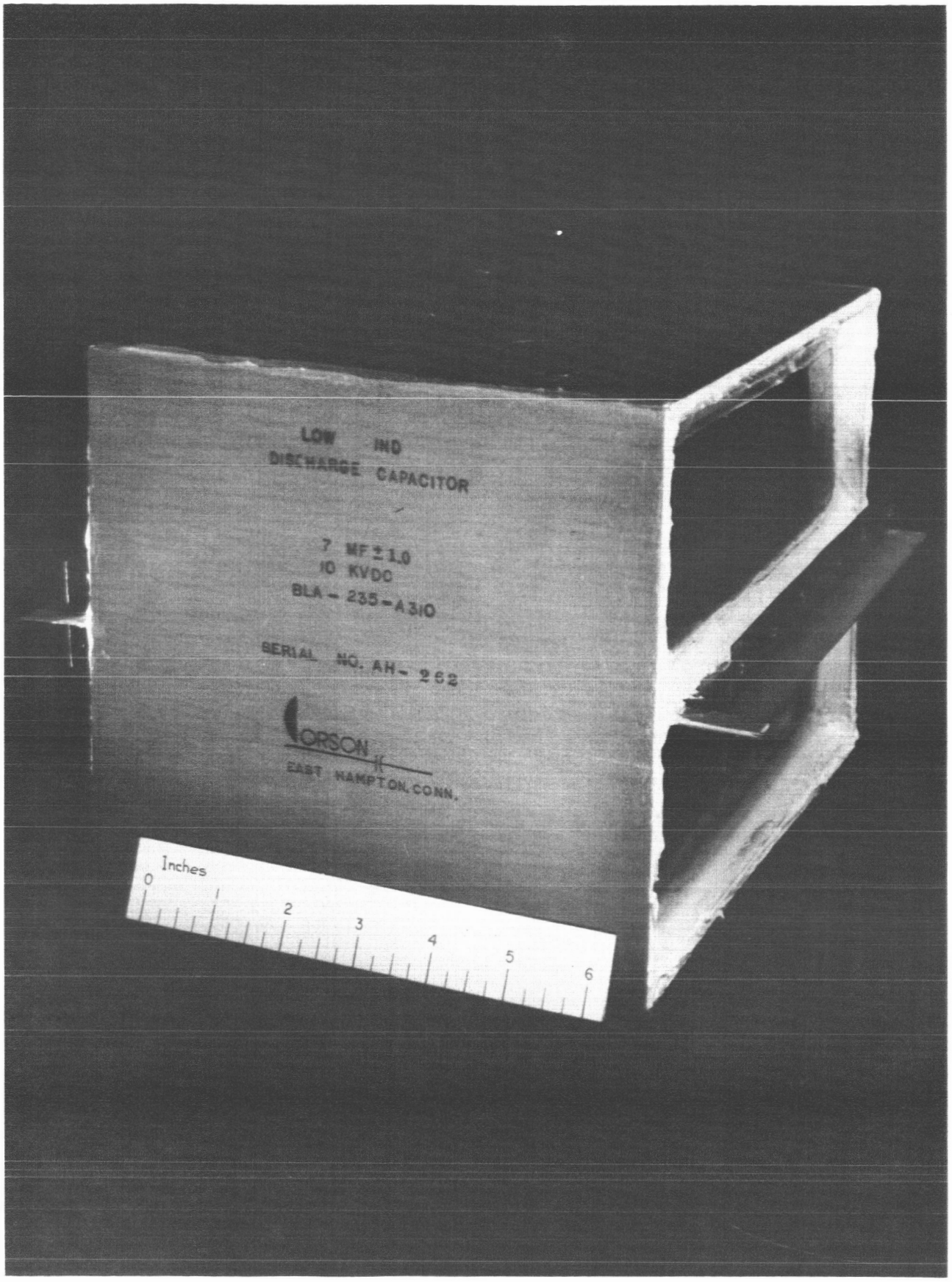

APZS-1264-66

PROTOTYPE 10KV CAPACITOR

FIGURE 31

VIII. PLASMA EXHAUST STUDIES (Clark-Eckbreth)

The study of the exhaust of a pulsed plasma from an orifice has been continued during this reporting period, but has primarily involved construction and calibration of more sophisticated diagnostic equipment which will facilitate more rapid and accurate data accumulation during the detailed program to follow. As noted in the previous semi-annual report[I-32] the most striking observation made in the preliminary studies was an apparent stabilization of the exhaust plume current pattern into a steady configuration over the last two thirds of a 20 μsec - 120 kiloampere pulse. Whether this was a consequence of the constraint imposed by the relatively small exhaust vessel used then, or a more basic property of the ejection process was the main question guiding the most recent work.

Exhaust studies have now been initiated in the large Plexiglas vacuum facility also discussed in the previous report, and certain tentative results can be quoted. Specifically, the discharge chamber has been driven with various rectangular pulse current waveforms: 120 kiloamps for 20 μsec, 60 kiloamp for 40 μsec, and 30 kiloamps for 80 μsec. Each pulse represents a fixed energy in the capacitor bank of about 6,500 joules. The back pressure in the tank has also been varied over the complete range from .02 μ to 100 μ of Argon using the shock tube gas injection triggering technique described earlier. The following trends have been observed in these studies:

1. For a given pulse time and current amplitude a greater portion of the arc current appears to flow into the exhaust plume at higher tank back pressures than at lower back pressures.

2. For a given energy pulse, a greater percentage of current appears to flow into the plume for longer pulse times than with shorter pulses.

3. At high back pressures the current distribution appears to stabilize in the exhaust plume; at low back pressures this stabilization has not yet been observed.

4. The current pattern propagates more rapidly through the plume, both axially and radially in the low back pressure cases than in the high pressure cases.

These preliminary studies are now being supplemented by more detailed and systematic probing of the exhaust. To accomplish this, the large Plexiglas facility has been equipped with a probe rake with axial and radial drives capable of handling 13 magnetic probes at one time and capable of supporting other types of probes (Fig. 32). In addition to this device, a 4" diameter Rogowski coil has been provided which is capable of surveying enclosed current on the axis of the exhaust vessel from the orifice to the far end of the tank; a voltage divider has been mounted across the electrodes; and various Faraday probes are under construction. Coupled with the existing photographic equipment, these will permit rapid, accurate survey of plume characteristics over a broad range of operating conditions, and hopefully will clarify the process of current stabilization and back pressure effects.

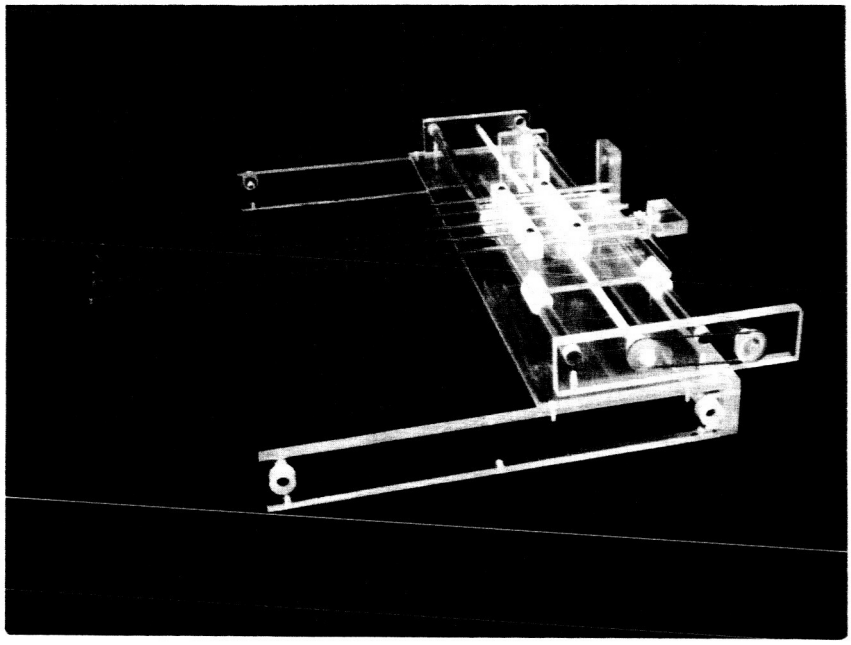

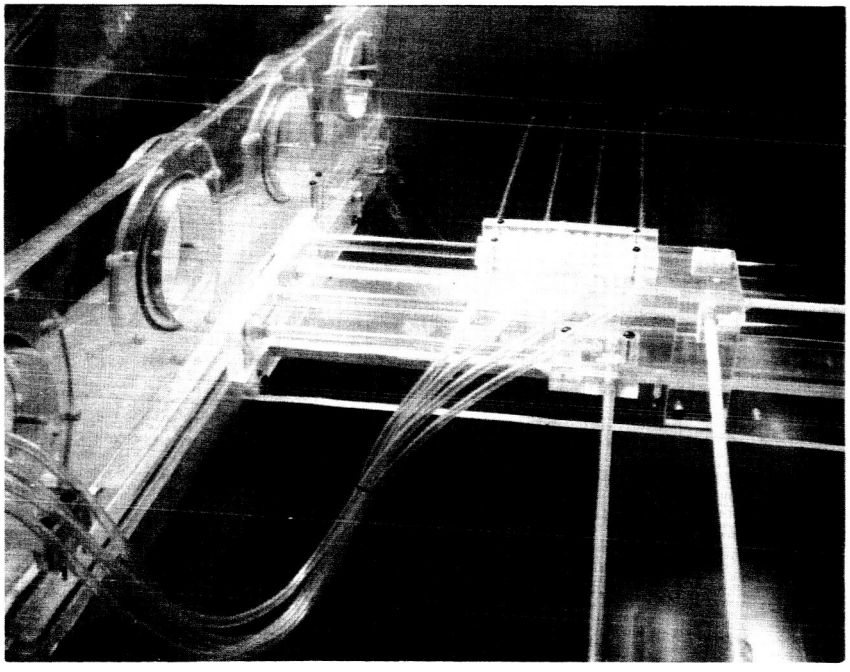

MULTIPLE PROBE ARRANGEMENT FOR PLEXIGLAS VACUUM TANK

AP25-P66-66

FIGURE 32

I. PROJECT REFERENCES

I-1. "Proposed Studies of the Formation and Stability of an Electromagnetic Boundary in a Pinch." Proposal for NASA Research Grant NsG-306-63, 5 March 1962.

I-2. First Semi-Annual Progress Report for the period 1 July 1962 to 31 December 1962, Research Grant NsG-306-63, Aeronautical Engineering Report No. 634, Princeton University, Princeton, New Jersey.

I-3. "The Plasma Pinch as a Gas Accelerator," AIAA Electric Propulsion Conference, 11-13 March 1963, Preprint No. 63013.

I-4. Second Semi-Annual Progress Report for the period 1 January 1963 to 30 June 1963, Research Grant NsG-306-63, Aeronautical Engineering Report No. 634a, Princeton University, Princeton, New Jersey.

I-5. "Structure of a Large-Radius Pinch Discharge," AIAA Journal 1, 8, 1809-1814, (1963).

I-6. "Gas-Triggered Inverse Pinch Switch," Review of Scientific Instruments 34, 12, 1439-1440 (1963).

I-7. "A Gas-Triggered Inverse Pinch Switch," Technical Note, Aeronautical Engineering Report No. 660, Princeton University, Princeton, New Jersey, August, 1963.

I-8. "Pulsed Electromagnetic Gas Acceleration," Paper No. II, 8, Fourth NASA Intercenter Conference on Plasma Physics in Washington, D. C., 2-4 December 1963.

I-9. "Current Distributions in Large-Radius Pinch Discharges," AIAA Aerospace Sciences Meeting, 20-22 January 1964, AIAA Preprint No. 64-25.

I-10. "Current Distributions in Large-Radius Pinch Discharges," AIAA Bulletin 1, 1, 12 (1964).

I-11. "Current Distributions in Large-Radius Pinch Discharges," AIAA Journal 2, 10, 1749-1753 (1964).

I-12. Third Semi-Annual Progress Report for the period 1 July 1963 to 31 December 1963, Research Grant NsG-306-63, Aeronautical Engineering Report No. 634b, Princeton University, Princeton, New Jersey.

I-13. "Pulsed Electromagnetic Gas Acceleration," Renewal Proposal for 15 months extension of NASA Research Grant NsG-306-63, Princeton University, Princeton, New Jersey, dated 15 January 1964.

I-14. Fourth Semi-Annual Progress Report for the period 1 January 1964 to 30 June 1964, Research Grant NsG-306-63, Department of Aerospace and Mechanical Sciences Report No. 634c, Princeton University, Princeton, New Jersey.

I-15. "Gas-Triggered Pinch Discharge Switch," Princeton Technical Note No. 101, Department of Aerospace and Mechanical Sciences, Princeton University, Princeton, New Jersey, July 1964.

I-16. "Gas Triggered Pinch Discharge Switch," The Review of Scientific Instruments 36, 1, 101-102 (1965).

I-17. "Double Probe Studies in an 8" Pinch Discharge," M.S.E. Thesis of J. M. Corr, Department of Aerospace and Mechanical Sciences, Princeton University, Princeton, New Jersey, September 1964.

I-18. "Exhaust of a Pinched Plasma from an Axial Orifice," AIAA Bulletin 1, 10, 570 (1964).

I-19. "Exhaust of a Pinched Plasma from an Axial Orifice," AIAA Second Aerospace Sciences Meeting, New York, New York, 25-27 January 1965, Paper No. 65-92.

I-20. "Ejection of a Pinched Plasma from an Axial Orifice," AIAA Journal 3, 10, 1862-1866 (1965).

I-21. Fifth Semi-Annual Progress Report for the period 1 July 1964 to 31 December 1964, Research Grant NsG-306-63, Department of Aerospace and Mechanical Sciences Report No. 634d, Princeton University, Princeton, New Jersey.

I-22. "On the Dynamic Efficiency of Pulsed Plasma Accelerators," AIAA Journal 3, 6, 1209-1210 (1965).

I-23. "Linear Pinch Driven by a High-Current Pulse-Forming Network," AIAA Bulletin 2, 6, 309 (1965).

I-24. "Linear Pinch Driven by a High Current Pulse-Forming Network," 2nd AIAA Annual Meeting, San Francisco, California, 26-29 July 1965, Paper No. 65-336.

I-25. "The Design and Development of Rogowski Coil Probes for Measurement of Current Density Distribution in a Plasma Pinch," M.S.E. Thesis of Edward S. Wright, Department of Aerospace and Mechanical Sciences, Princeton University, Princeton, New Jersey, May 1965.

I-26. "The Design and Development of Rogowski Coil Probes for Measurement of Current Density Distribution in a Plasma Pinch," Department of Aerospace and Mechanical Sciences Report No. 740, Princeton University, Princeton, New Jersey, June 1965.

I-27. "Pulsed Electromagnetic Gas Acceleration," Renewal Proposal for 12 months extension of NASA Research Grant NsG-306-63, Princeton University, Princeton, New Jersey, dated 7 June 1965.

I-28. "Miniature Rogowski Coil Probes for Direct Measurement of Current Density Distributions in Transient Plasmas," The Review of Scientific Instruments 36, 12, 1891-1892 (1965).

I-29. Sixth Semi-Annual Progress Report for the period 1 January 1965 to 30 July 1965, Research Grant NsG-306-63, Department of Aerospace and Mechanical Sciences Report No. 634e, Princeton University, Princeton, New Jersey.

I-30. "Cylindrical Shock Model of the Plasma Pinch," M.S.E. Thesis of Glen A. Rowell, Department of Aerospace and Mechanical Sciences, Princeton University, Princeton, New Jersey, February 1966.

I-31. "Cylindrical Shock Model of the Plasma Pinch," Department of Aerospace and Mechanical Sciences Report No. 742, Princeton University, Princeton, New Jersey, February 1966.

I-32. Seventh Semi-Annual Progress Report for the period 1 July 1965 to 31 December 1965, Research Grant NsG-306-63, Department of Aerospace and Mechanical Sciences Report No. 634f, Princeton University, Princeton, New Jersey.

I-33. "Electric and Magnetic Field Distributions in a Propagating Current Sheet," AIAA Bulletin 3, 1, 35, (1966).

I-34. "Electric and Magnetic Field Distributions in a Propagating Current Sheet," AIAA Fifth Electric Propulsion Conference, San Diego, California, 7-9 March 1966, Paper No. 66-200.

I. PROJECT REFERENCES - CONTD.

I-35. "Pulse Forming Networks for Propulsion Research," Paper presented at the Seventh Symposium on Engineering Aspects of Magnetohydrodynamics, Princeton University, Princeton, New Jersey, March 30-April 1, 1966 (p. 10-11 of Symposium Proceedings).

I-36. "Dynamics of a Pinch Discharge Driven by a High Current Pulse Forming Network," Ph.D. Thesis of Neville A. Black, Department of Aerospace and Mechanical Sciences, Princeton University, Princeton, New Jersey, May 1966.

I-37. "Dynamics of a Pinch Discharge Driven by a High Current Pulse-Forming Network," Aeronautical Engineering Report No. 778, Department of Aerospace and Mechanical Sciences, Princeton University, Princeton, New Jersey, May 1966.

I-38. "Pulsed Plasma Propulsion," Paper presented at the Fifth NASA Intercenter and Contractors Conference on Plasma Physics, Washington, D. C., 24-26 May 1966, p. 75-81, Part V of Proceedings.

I-39. "Pulsed Electromagnetic Gas Acceleration," Renewal Proposal for 24 months extension of NASA Research Grant NsG-306-63, Princeton University, Princeton, New Jersey, 25 May 1966.

I-40. "A Large Dielectric Vacuum Facility," AIAA Journal 4, 6, 1135, (1966).

I-41. "Structure of the Current Sheet in a Pinch Discharge," Ph.D. Thesis of Rodney L. Burton, Department of Aerospace and Mechanical Sciences, Princeton University, Princeton, New Jersey, August 1966.

II. GENERAL REFERENCES

II-1. Jahoda, F. C., Little, E. M., Quinn, W. E., Ribe, F. L. and Sawyer, G. A., "Plasma Experiments with a 570-KJ Theta-Pinch," Journal of Applied Physics, 35, 8, 2351 (1964).

II-2. Ashby, D. E. T. F. and Jephcott, D. F., "Measurement of Plasma Density Using a Gas Laser as an Infrared Interferometer," Applied Physics Letters, 3, 1, 13 (1963).

II-3. Wheeler, C. B. and Dangor, A. E., "Laser Interferometric Measurements of Rapid Electron Density Changes in a Plasma," Paper No. 2, Session VII, 26th Meeting of the NATO AGARD Propulsion and Energetics Panel in Pisa, Italy, 6-10 September 1965.

II-4. Verdeyen, J. T. and Gerardo, J. B., "Plasma Diagnostics with Gas Lasers," Paper No. 3, Session VII, 26th Meeting of the NATO AGARD Propulsion and Energetics Panel in Pisa, Italy, 6-10 September 1965.

II-5. Gerardo, J. B., Verdeyen, J. T. and Gusinow, M. A., "High-Frequency Laser Interferometry in Plasma Diagnostics," Journal of Applied Physics, 36, 7, 2146 (1965).

APPENDIX A:

Semi-Annual Statement of Expenditures

PULSED ELECTROMAGNETIC
GAS ACCELERATION
Grant NsG-306-63

1 January 1966 - 30 June 1966

Direct Costs

I.	Salaries and Wages		
	A. Professional	$ 10,500	
	B. Students	4,301	
	C. Technicians	7,050	
	D. Supporting Staff	7,915	$ 29,766
II.	Employee Benefits (12% of Item I)		3,572
III.	Equipment		450
IV.	Materials and Services		5,649
V.	Communications and Shipping		-
VI.	Travel		1,916
	Total Direct Costs		$ 41,353

Indirect Costs

VII.	Overhead (20% of Items I thru V)	8,270
	Total Costs	$ 49,623